

# Design and Constraints of the *Drosophila* Segment Polarity Module: Robust Spatial Patterning Emerges from Intertwined Cell State Switches

GEORGE VON DASSOW<sup>1,2\*</sup> AND GARRETT M. ODELL<sup>1,2</sup>

<sup>1</sup>Department of Zoology, University of Washington, Seattle, Washington 98105

<sup>2</sup>Friday Harbor Laboratories, Friday Harbor, Washington 98250

**ABSTRACT** The *Drosophila* segment polarity genes constitute the last tier in the segmentation cascade; their job is to maintain the boundaries between parasegments and provide positional “read-outs” within each parasegment for the entire developmental history of the animal. These genes constitute a relatively well-defined network with a relatively well-understood patterning task. In a previous publication (von Dassow et al. 2000. *Nature* 406:188–192) we showed that a computer model predicts the segment polarity network to be a robust boundary-making device. Here we elaborate those findings. First, we explore the constraints among parameters that govern the network model. Second, we test architectural variants of the core network, and show that the network tolerates a wide variety of adjustments in design. Third, we evaluate several topologically identical models that incorporate more or less molecular detail, finding that more-complex models perform noticeably better than simplified ones. Fourth, we discuss two instances in which the failure of the network model to behave in a life-like fashion highlights mechanistic details that need further experimental investigation. We conclude with an explanation of how the segment polarity network can be understood as an interwoven conspiracy of simple dynamical elements, several bistable switches and a homeostat. The robustness with which the network as a whole maintains a spatial regime of stable cell state emerges from generic dynamical properties of these simple elements. *J. Exp. Zool. (Mol. Dev. Evol.)* 294:179–215, 2002. © 2002 Wiley-Liss, Inc.

A decade ago most developmental biologists worked in the context of “developmental pathways,” ordering developmental control genes into chains of regulatory events contributing to the eventual phenotype. The prevailing image of the developmental process evolves to keep up with new information, and increasingly, biologists think about developmental and molecular genetics in terms of networks of dynamic gene interactions characterized by extensive internal crosstalk and feedback. While this subtle change is surely toward a more realistic conception of gene function, it poses a potentially serious problem, since highly integrated dynamical networks are much harder to understand, mechanistically, than are top-down processes like pathways and cascades. This is emphasized by a contrast between two simple maps of gene interactions in Figure 1. In Figure 1A, published earlier (von Dassow et al., '93), it is trivial to evaluate what the map, to the extent that it reflects reality, does: either the signals at the top are strong enough, and the connections sufficiently strong, too, to generate an output at the bottom, or they are not. On the other

hand, in a slightly later paper, the same authors (Schmidt et al., '96) presented Figure 1B, in which it is essentially impossible to tell, just from the map alone, *what the network does*. One correctly suspects that the behavior of this circuit depends on dynamical parameters, such as the relative strengths of the various connections composing the map, or the initial state of the components, etc.

Another subtle shift epitomized in Figure 1 is that the phenotypic consequences of gene activity seem to have evaporated in Figure 1B. Instead of characterizing the functions of genes and their products in terms of the production of a developmental event or a specific tissue type (as in Fig. 1A), there is an implicit focus on the gene network as a device in and of itself (Hartwell et al., '99; von Dassow and Munro, '99). The more biologists know about a particular mechanism,

Grant sponsor: National Science Foundation; Grant numbers: MCB-9732702, MCB-9817081, MCB-0090835.

\*Correspondence to: George von Dassow, Friday Harbor Laboratories, Friday Harbor, WA 98250. E-mail: dassow@u.washington.edu.

Received 19 September 2001; Accepted 10 June 2002.

Published online in Wiley InterScience (www.interscience.wiley.com). DOI: 10.1002/jez.10144

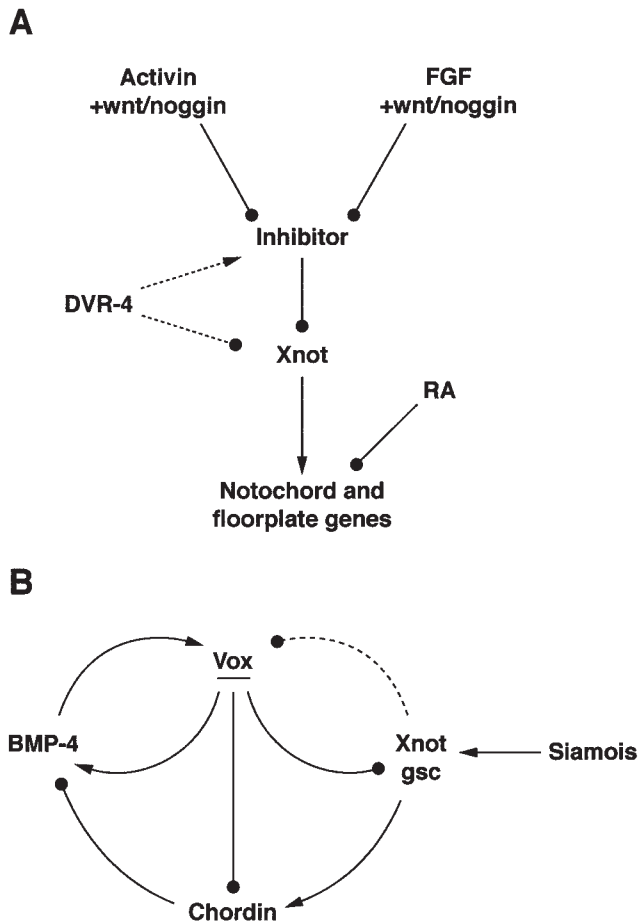


Fig. 1. Examples of evolving views of genetic regulatory architecture. (A) Diagram from von Dassow et al. ('93), representing the “genetic cascade” or “developmental pathway” type of thinking necessitated when the task is to order just a few known components relative to a particular phenotype. (B) Later diagram from the same authors (Schmidt et al., '96) captures a nascent “gene network” notion, stimulated when enough feedback and cross-talk made the “pathway” metaphor inappropriate.

the more the functions of individual genes and their products get re-defined in terms of the way they contribute to intrinsic dynamical behaviors of the network, whose function is in turn related to how that intrinsic behavior is deployed in the three-dimensional context of the developing embryo. But again, it is *not* possible to answer, using words and intuition alone, *what is the intrinsic dynamic behavior of this network?* An obvious corollary is that it is also impossible to say, using intuition alone, whether the map in Figure 1B *actually accounts for any real phenomenon*. In this paper we describe a theoretical study in which we use a computer simulation model of the segment polarity network in early *Drosophila* development

to explore a set of hypotheses about the nature and function of that network. Brief reports on this work appeared previously (von Dassow et al., 2000) and in a companion paper (Meir et al., 2002b, this issue); here we expand and extend those results to suggest that the segment polarity network is a boundary maintaining module that exhibits remarkable robustness of its steady-state pattern forming behavior to structural, dynamic, and architectural perturbations.

## PARAMETER SPACE AS A BIOLOGICAL PROBLEM

Consider a simplistic example: two genes activating each other (Fig. 2A). Figure 2B exhibits the simplest plausible formulation of this circuit's dynamics: the differential equations say that the rate of change in concentration of each gene product depends on a dose–response curve in which the other gene product appears and a first-order decay term. In this simple case we can assess the behavior of the network by setting the left-hand sides to 0, and plotting the resulting curves (“nullclines”; Fig. 2C). Where the nullclines cross, the system is at steady state; Figure 2C shows that under some conditions there may

Fig. 2. Two-activator switch. (A) Two molecular species X and Y promote each other's synthesis, and each exhibits first-order decay. For such a simple system one may solve graphically for steady states. (C–F) are plots of nullclines for the equations in B; each curve is obtained by setting the derivative to zero and solving for the state variable governed by that equation. Where the curves cross in the state space, both derivatives are zero. However, such steady-state points may or may not be stable, as determined by the eigenvalues of the Jacobian matrix for the differential equations. For certain choices of parameters, there may be three steady states, only two of which are stable (dashed circles, large graph): one in which both species are expressed at high level, and one in which neither is expressed. In this case, the system behaves like a switch: for some initial conditions, it evolves deterministically toward one stable steady state, stays there, and returns after small perturbations; for some other initial conditions, it evolves toward the other stable state and stays there; and large perturbations can “switch” the system to one or the other stable state. However, the stability and even the existence of each state depends on the choice of values for free parameters. D and E show that switch-like behavior depends critically on sigmoid dose–response behavior; if the parameter  $v=1.0$ , there is no way this system can exhibit switching. Either the nullclines cross, and only the “on” state is stable, or they do not, and only the “off” state is stable. In F, despite that  $v > 1.0$ , the parameters  $K_X$  and  $K_Y$  are such that the nullclines happen not to cross, and only the “off” state is stable.

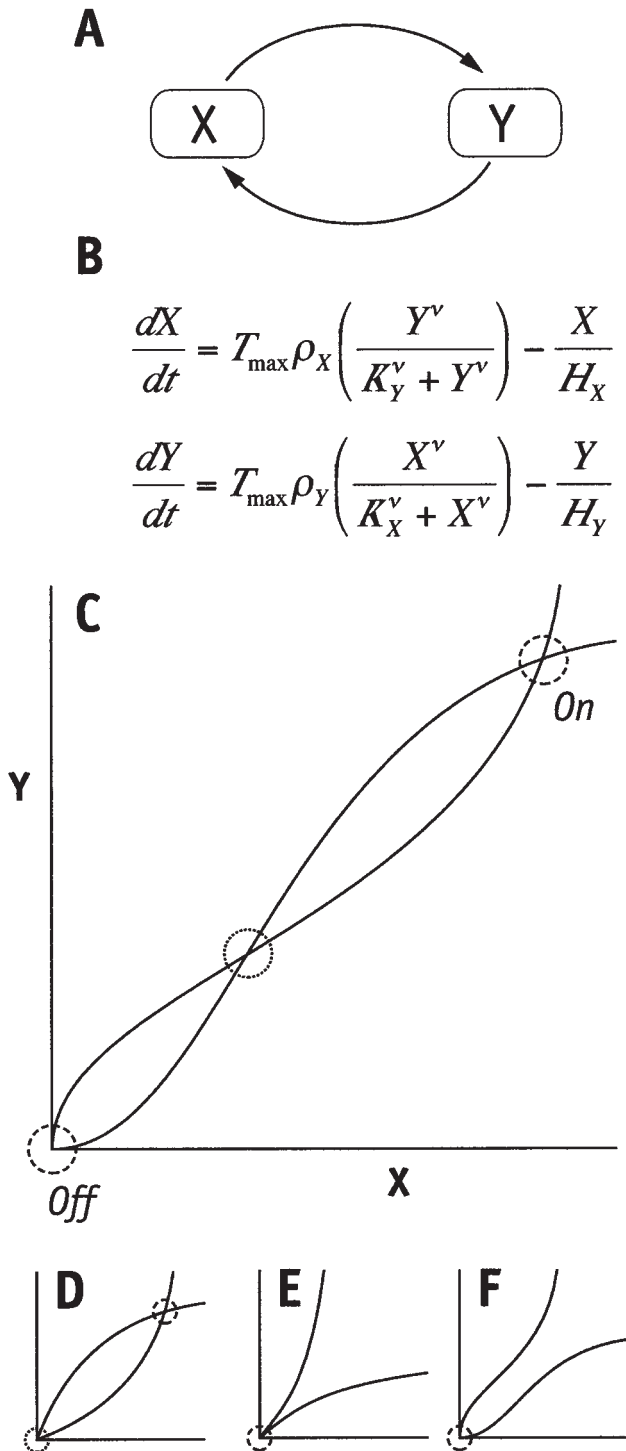
exist three steady-state points, two of which are stable (that is, the system tends to return to those points if nudged away from them), in which case this tiny circuit could function as a switch; if pushed near one or the other stable steady state (“Off” or “On” in this case), it will evolve toward

and remain at that state until perturbed into the neighborhood (attraction basin) of the other stable steady state. This switch-like behavior exemplifies the dependence of the circuit’s behavior on initial conditions.

However, the switch-like behavior itself depends intimately on the values of several free parameters. The equations in Figure 2B involve nine free parameters, which represent empirically measurable values governing the dynamics, such as the half-life of each molecular species, the maximal transcription rate, etc. Parameters could themselves be functions of other genes extrinsic to the putative module of interest, or they may be functions of temperature and other environmental variables, etc., but with respect to the intrinsic behavior of the circuit in question they are constants whose values must be specified somehow. As shown in Figure 2D–F, under some parameter conditions the switch-like behavior is completely abolished. Therefore, although the dynamical argument confirms that the circuit in Figure 2B *could* function as a switch, there is no way to tell, from the network’s topology alone, if it actually *does*.<sup>1</sup> If such a simple device as the two-activator switch is so problematic, imagine how useless topology alone becomes when confronted with networks only a little bit more complex, such as Figure 1B.

This is not a mere mathematical pet peeve; it has a genuinely important biological meaning. We can think of the free parameters of a network as the basis for a space (a nine-dimensional space in the case of Fig. 2) which the network inhabits. Each point in that space is a unique set of values for each free parameter. Given a functional behavior for the network, some subset of points in parameter space (which for any realistic module will have dozens of axes) might confer that behavior, and the questions become *in what fraction of parameter space does the circuit “work,”* and *how are the working parameter sets distributed in that space?* Some simple possibilities are stereotyped in Figure 3: the fraction could be large, in which case we would say that the network, or rather the behavior in question, is robust to parameter variation, whereas if the fraction of working territory is small, we would say it is brittle. *Moreover, the evolutionary process*

<sup>1</sup>In fact, the situation is really even a little worse: in general it will be impossible to use formulations like these to answer *whether* a given set of known facts about epigenetic relations really does account for a particular behavior; instead it is only possible to ask *whether there exists any set of parameters for which those facts could do so*.



itself has to find the working territory, and, having found it, it needs to stay within it. Since parameters are themselves mutable functions of the gene products involved in the network, as well as possibly others extrinsic to it, mutation constantly disperses the network through parameter space. Thus the evolutionary process must confront a variety of consequences of how the network resides in parameter space.

### THE SEGMENT POLARITY NETWORK

Dozens of man-millennia have gone into dissecting segmentation in the fruit fly *Drosophila*. While understanding of this process remains incomplete, segmentation in the *Drosophila* embryo ranks among the very best-understood of all developmental mechanisms. The segmentation process consists of a series of ever-finer-scale patterning processes, beginning with morphogens

localized in the egg during oogenesis (summarized in Fig. 4, following a similar diagram presented by Nagy, '98; the diagram is meant only to convey the flavor of the process). Maternal morphogens like *bicoid* and *nanos* form shallow gradients along the future A-P axis of the embryo. Gap genes respond to the local concentration of these factors and also regulate each other's production, and the functional pattern of expression of these genes is broad bands with moderate-range gradients for each shoulder. Pair-rule genes respond, in turn, to the local concentration of gap gene products, and their functional expression patterns typically correspond to alternate segments, with short-range gradients for shoulders. Many of the gap and pair-rule genes are expressed initially in broad domains, and their functional expression patterns emerge through repression by other gap and pair-rule genes (Gaul and Jackle, '87; Edgar et al., '89; Carroll, '90; Kraut and Levine, '91). The segmental register of most pair-rule gene expression patterns implies that it is, in effect, these genes that map out segments at the blastoderm stage.

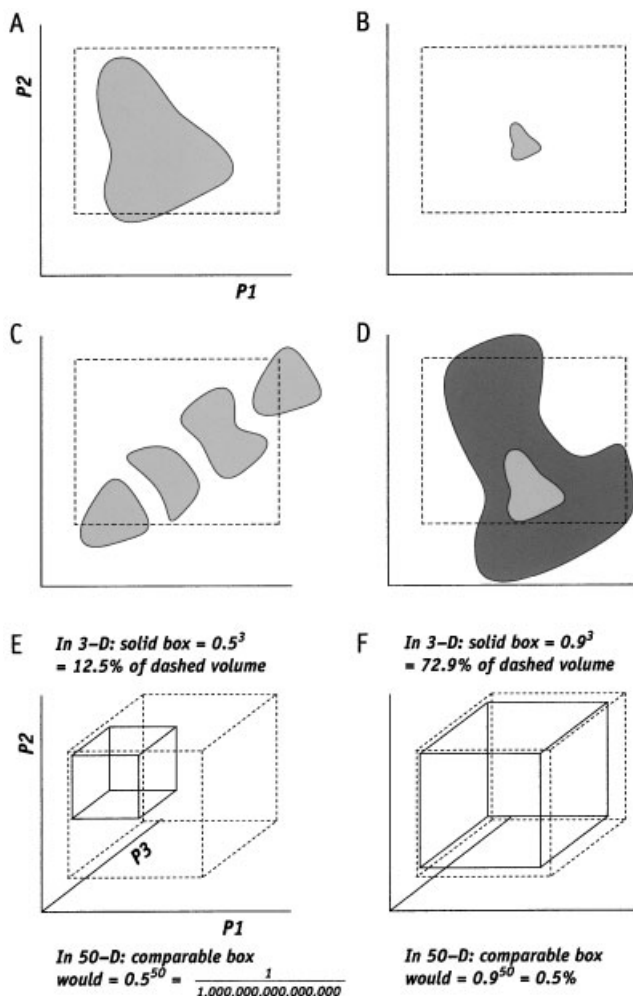


Fig. 3. A few possible configurations of functional domains in parameter space. In each panel the dashed box indicates a boundary within which one might wish to search for "functional" sets of parameter values. In (A) a large fraction of parameter choices confer function (the shaded lake). In (B) the model is limited to a tiny puddle. One might find that the model functions in several disjoint regions of parameter space, as in C. Finally, in (D), a smallish functional pond is surrounded by a much larger swamp of almost-functional values (darker shading), which might even smoothly grade into the fully functional region; in such a case one could use optimization strategies to find the functional pond as long as one stumbled first into the massive slough surrounding it. In A the working territory occupies about one-third the "volume" of the sampled region, whereas in B the working territory occupies more like one-fiftieth. For a realistic gene network model, the reader must extrapolate to high dimensionality—say, 50 dimensions, as for our core segment polarity model. As shown in E, if one contiguous half of each parameter axis within the sampled range were compatible with the desired function, in a three-dimensional parameter space one-eighth of the sampled volume would "work," but the equivalent box in 50-D space would occupy a minuscule fraction of the sampled volume. (F) For the core segment polarity model we found that about one in 200 randomly sampled parameter sets work; the equivalent box in a 3-D parameter space would occupy nearly the entire sampled volume. The rectangular prisms in E and F are meant only to express the volume fraction, not the complex shape, of the zone that the functional parameter sets occupy in parameter space.

However, most of the pair-rule genes are only transiently expressed, and it is the next tier in the segmentation cascade, the segment polarity network, that defines and maintains the boundaries between segments. The segment polarity genes respond to the local combination and concentrations of pair-rule gene products, and they come to be expressed in narrow stripes in every segment (reviewed by Martin-Arias, '93; DiNardo et al., '94). Their expression patterns, though more dynamic than this crude character-

ization implies, remain landmarks for the segmental boundary in at least a subset of the embryo (especially the ventral ectoderm) throughout embryogenesis and into the adult (via their role in maintaining the A-P compartment boundary in imaginal discs). The segment polarity network includes: *engrailed* (*en*) and its duplicate *invected* (*inv*), which encode transcriptional regulators expressed posterior to the parasegmental boundary (DiNardo et al., '88; Martinez-Arias et al., '88); *hedgehog* (*hh*), which encodes a signaling molecule expressed under the control of Engrailed (Tabata et al., '92); *wingless* (*wg*), which encodes another signaling molecule expressed anterior to the parasegmental boundary (Martinez-Arias et al., '88; van den Heuvel et al., '89); *patched* (*ptc*), which encodes the inhibitory and Hh-binding component of the Hh receptor (Hooper and Scott, '89; Chen and Struhl, '96; Marigo et al., '96; Alcedo and Noll, '97; Chen and Struhl, '98); *cubitus interruptus* (*ci*), a fascinatingly complex transcriptional regulator that mediates the response to Hh signaling (Orenic et al., '90; Schwartz et al., '95; Alexandre et al., '96; Dominguez et al., '96; Aza-Blanc et al., '97; Hepker et al., '97; Von Ohlen et al., '97; Chen et al., '98; Ohlmeyer and Kalderon, '98; Wang and Holmgren, '99); *smoothened* (*smo*), *fused* (*fu*), *costal* (*cos*), *Suppressor of fused* (*Su(fu)*), all components of the Hh signaling pathway (Alcedo et al., '96; van den Heuvel and Ingham, '96; Sisson et al., '97; Alves et al., '98; Monnier et al., '98); *frizzled* (*fz*) and *Dfrizzled2* (*Dfz2*), *dishevelled*

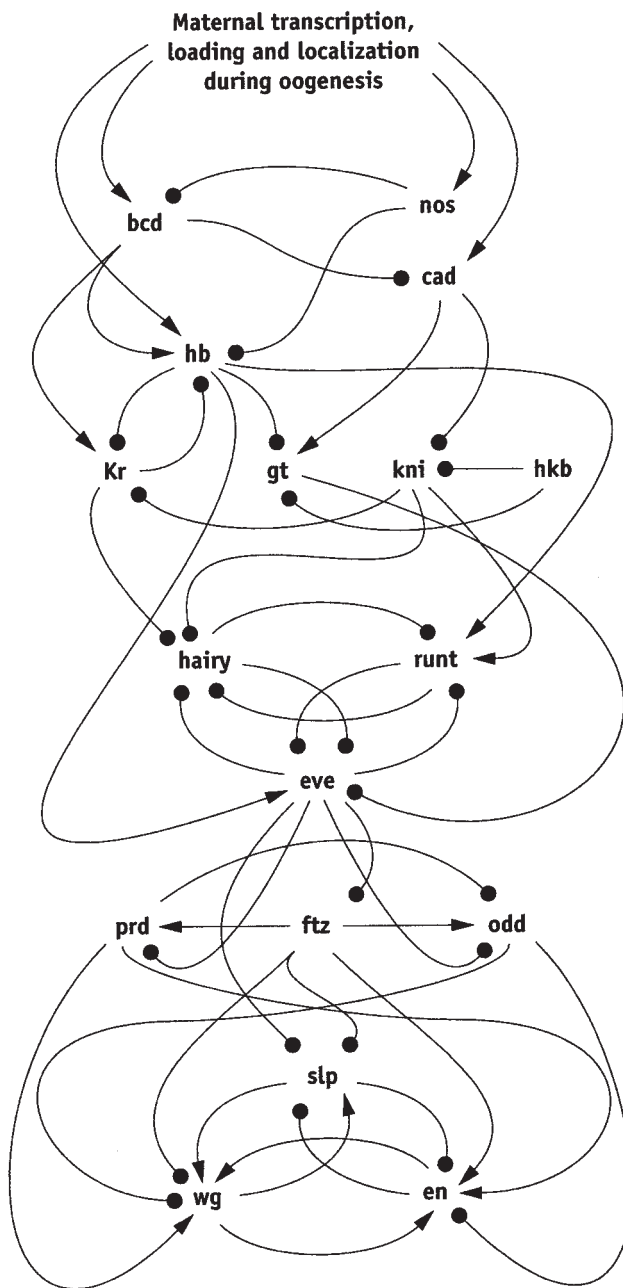


Fig. 4. A conceptual summary of the *Drosophila* segmentation cascade. Redrawn after a figure of Lisa Nagy's ('98), and embellished according to various sources, especially the "blue book" chapters on segmentation (especially Martinez-Arias, '93). This diagram, which is incomplete and inaccurate, is only intended to convey the overall gist of the process, as outlined in the main text. The graphical design is meant to convey that the segmentation cascade consists of a series of interwoven cassettes. The members of each cassette interact strongly with each other and have strong influences on members of downstream cassettes but little if any influence on upstream cassettes. This diagram is especially misleading with regard to the interface between the gap genes and the primary pair-rule genes, and with regard to interactions among pair-rule genes. In reality, gap genes exert complex stripe-specific regulatory control over the pair-rule genes, and may repress a given gene in one region while activating it in another. This is achieved through the use of quasi-independent enhancer regions for each *hairy* or *eve* stripe. Finally, of course, the segment polarity network is not adequately represented in this figure at all!

(*dsh*), *shaggy* (*sgg*), *naked* (*nkd*), *armadillo* (*arm*), and *pangolin* (*pan*), all components of wingless signal transduction (Brunner et al., '97; Cadigan and Nusse, '97; van de Wetering et al., '97; Bhat, '98; Bhanot et al., '99); and other genes including *gooseberry* (*gsb*) (Li and Noll, '93) and *sloppy-paired* (*slp*) (Grossniklaus et al., '92; Cadigan et al., '94b). The *en*- and *wg*-expressing domains are initially set up by the pair-rule genes (Ingham et al., '88), but as pair-rule expression fades out, *en* and *wg* become dependent on one another, before eventually locking into various autoregulatory loops (DiNardo et al., '88; Heemskerk et al., '91; Vincent and O'Farrell, '92; Li and Noll, '93; Hooper, '94; Vincent and Lawrence, '94; Yoffe et al., '95) that, in a subset of embryonic tissues, maintain the compartmentalization of segments and the expression of the segment polarity genes throughout development. To summarize, gap and pair-rule genes encode transcription factors that are transiently expressed during segmentation; in contrast, the segment polarity genes encode a variety of transcription factors, secreted cell signaling factors, receptors, transducers, cytoskeletal components, etc., and they are stably expressed throughout development.

We became interested in the segment polarity network because of the tempting possibility that this group of genes might qualify as a developmental "module" (von Dassow and Munro, '99) that the evolutionary process has repeatedly dissociated from its inputs and outputs as it has been redeployed in various developmental contexts. Current evidence tentatively *suggests* on the basis of the conserved expression of *engrailed* homologues (Patel et al., '89; Patel, '94; Rogers and Kaufman, '96; Grbic et al., '98; Peterson et al., '98), and a few experiments testing the regulatory relationship between *wingless* and *en* (Nagy and Carroll, '94; Oppenheimer et al., '99) suggest that the segment polarity network may be involved in segmentation in all insects, perhaps all arthropods.

The same is apparently *not* true of the gap and pair-rule genes that, in *Drosophila*, provide the initial inputs to the segment polarity network. Essentially all insects (excepting certain polyembryonic forms) begin embryogenesis as a syncytium in which the hundreds or thousands of nuclei share the cytoplasm and thus interact without the need (or possibility) of cell-cell communication (Anderson, '73). The gap and pair-rule networks, as we know them in *Drosophila*, as well as the

maternal morphogens, depend on the syncytial context of segmentation. However, only long-germ insects, including the flies, bees, and some beetles, specify all body segments while nuclei share a common cytoplasm. Short-germ insects such as the locusts specify only a few segments while syncytial; the rest emerge sequentially from a cellular growth zone at the posterior of the embryo. Perhaps the ancestral condition was something like the intermediates of today, such as the dragonflies and many of the bugs and beetles, in which about half the segments form in the syncytium, and the rest in a cellular context (Patel, '94; Tautz et al., '94). Homologues of gap and pair-rule genes exist in extreme short-germ insects like grasshoppers, and some, but not all, of these are expressed in patterns that imply roles in segmentation even during post-cellularization segment formation (e.g., Patel et al., '92, 2001; Sommer and Tautz, '93; Dawes et al., '94; Brown et al., '94, '97; Dearden and Akam, 2001). However, it seems unlikely that the gap and pair-rule networks, to whatever extent they are involved in post-cellularization segmentation, function the same way as they do in *Drosophila* to provide the upstream pre-patterning for the segment polarity network, simply because, again, the known mechanism by which these two groups of genes' expression patterns emerge depends on the absence of cell boundaries. Thus, it appears that the segment polarity network has retained its role in maintaining the segmental boundary despite a dramatic change in the very nature of the upstream patterning mechanisms from which it takes its prepattern.

Moreover, the segment polarity network, or subsets thereof, is used in a variety of different organisms to do a variety of different patterning tasks. In the most dramatic example, the primordium of the butterfly eyespot expresses several of the core segment polarity genes in a spatial regime at least superficially distinct from their segmental patterns (Keys et al., '99). Since the eyespot is a novel adaptation within the Lepidoptera, it is hard to escape the conclusion that the evolutionary process somehow managed to re-deploy the segment polarity network at some point in the invention of the eyespot.

Thus, the questions we sought to answer, using a computer simulation model, were as follows: is our map of the segment polarity network complete enough to explain how, in the developing fly, it "remembers" a transient patterning imprint conferred by the pair-rule genes? Do the known

interactions among segment polarity genes account for the apparent modularity of the segment polarity network? What properties emerge from the conspiracy of these genes, that we could not have anticipated from descriptions of the parts alone?

**SYNOPSIS OF OUR PRIOR WORK ON THE SEGMENT POLARITY MODEL**

In a previous report (von Dassow et al., 2000) we showed that a model encompassing core interactions of the segment polarity network (Fig. 5B) could mimic patterns of gene expression observed in living embryos (Fig. 5A). Not only does this core network have this capacity, it is highly robust to variation in both parameter values and initial prepattern. In the jargon of dynamical systems theory, the network is both structurally and dynamically stable. We thus concluded that the facts embodied in the model suffice to explain the canonical phenomenology of the segment polarity network: namely, the stable maintenance of two stable cell states on either side of the parasegmental boundary, with a ground state occupying the rest of the segment. Furthermore, because the

core network can accomplish this task without any persistent, extrinsic spatial or temporal biases on any of its components, and because it can do so starting from a wide variety of initial conditions, we concluded that the segment polarity network qualifies as a developmental module.

That is, *the segment polarity network is a device unto itself*. It has certain intrinsic behaviors. Those behaviors may be selected among either by treating kinetic parameters as tuning dials, or by triggering the module with different prepatterns. Most remarkably, despite this tunability, the network is usually so robust that only very large turns of the metaphorical dials tune the network to different behaviors. But on the other hand, it is this very robustness that allows the network to move around in parameter space, varying its behavior upon the fundamental theme. Another way of looking at it is that while the core topology of the segment polarity network insulates its dynamical behaviors from subtle, quantitative perturbations, gross qualitative perturbations alter its behavior, often (nearly) discontinuously.

This simple model (hereafter the “core network,” “core model,” or “spg1”), because of the

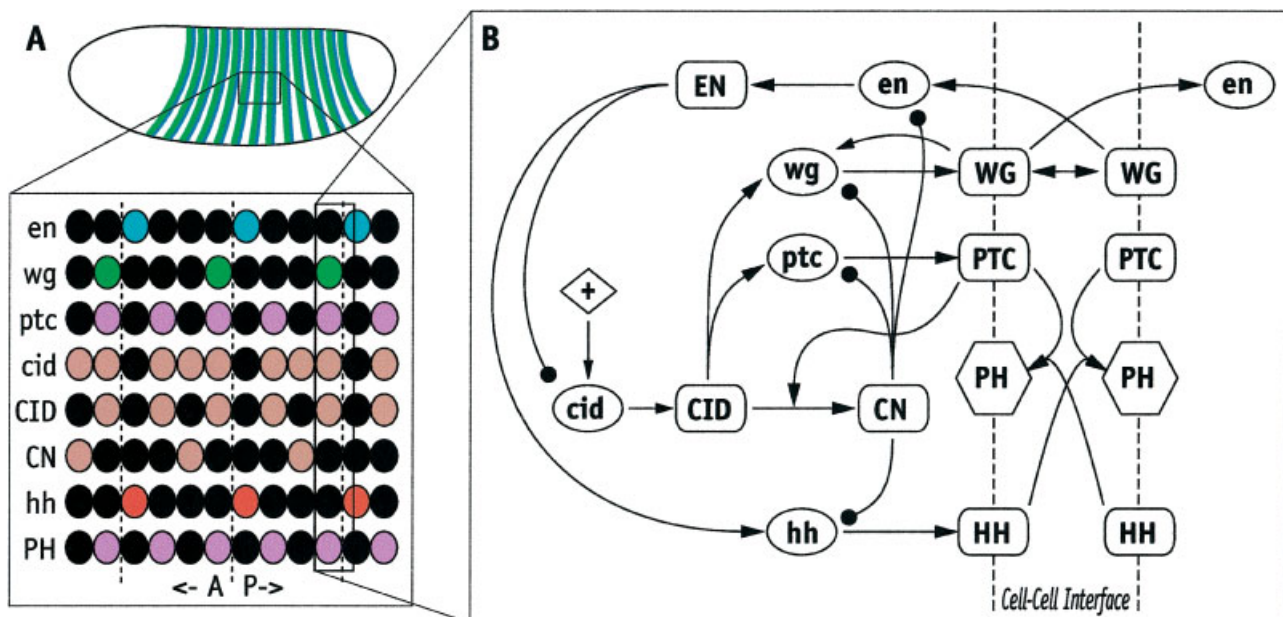


Fig. 5. Core segment polarity network and its task. Redrawn from von Dassow et al. (2000). (A) By the time the *Drosophila* embryo gastrulates, the segmentation cascade has mapped out all the borders between the developmental units known as “parasegments”; boundaries between parasegments are defined by the expression of *wg* to the anterior (green) and *en* to the posterior (blue). As development

proceeds the expression patterns of other segment polarity genes emerge, and we have stereotyped some of the central players as show. (B) Core segment polarity network described in von Dassow et al. (2000), which we found was the minimal realistic network capable of mimicking the stereotyped pattern shown in A.

brevity of its treatment to date, raises a variety of questions. Testing these issues and the development of more complex models provided several intriguing surprises. This paper tells the rest of the story, divided into four sections intended to be readable on their own. First, we analyze the distribution of working parameter sets in parameter space, and show that within a single, large sub-region working parameter sets are very common. Second, we test several topological variants of the original segment polarity model to show that the robustness of the model is not contingent on a particularly lucky subset of known interactions. Third, we contrast versions of the model with greater or lesser complexity, and show that, to our surprise, increasing the level of detail actually *improves* the robustness of the model. And, finally, we show that challenging the model with a dynamical patterning test imposes serious constraints on either details of the mechanism or the relative values of certain parameters.

## RESULTS AND DISCUSSION

### Section I: Constraints among parameters

For the core segment polarity model, we showed previously (von Dassow et al., 2000) that for essentially any value of most parameters, some choice of values for the other parameters allows the core network to perform its basic pattern-holding task (such a set of values we call a “solution”). However, it remains unclear whether there exist trade-offs among parameters or biases on the distribution of working values in parameter space. To explore this we tested 235,000 randomly chosen parameter sets among which we found 1,120 solutions, chosen from the same bounds used in our earlier work (see Supplementary Information for von Dassow et al., 2000), and then plotted solution frequency versus value for all parameters (Fig. 6). While for many parameters (most half-lives and cooperativity coefficients, primarily) the search returns an essentially flat distribution, for an important subset the distributions are moderately to strongly biased. This is the case for most of the parameters governing thresholds (half-maximal coefficients) for the activities of regulators with respect to their targets.

For example, Figure 6, column 1, row 4, shows that solutions are most abundant when the full-length Ci protein is only a weak activator of *wingless* transcription. Figure 6, column 1, row 5, shows that solutions are far more common if the

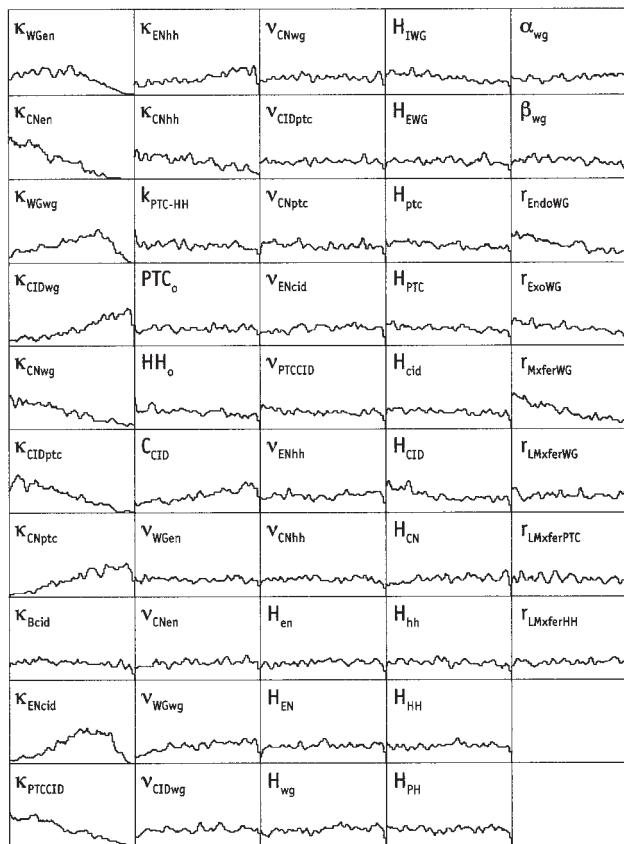


Fig. 6. Parameter distributions for the core segment polarity network model. Each cell of the table is a histogram; the horizontal axis is the entire range for the named parameter, and the vertical axis is the number of solutions that have a particular value. Parameter names follow the following conventions: “ $\kappa$ ” indicates a half-maximal activity coefficient; “ $v$ ” a cooperativity coefficient; “ $H$ ” a half-life (which is actually a time constant); “ $r$ ” indicates a first-order rate constant and “ $k$ ” a second-order constant; the subscript indicates which interaction the parameter in question governs, so “ $\kappa_{Xy}$ ” means the half-maximal activity of X with respect to activation of y transcription; “X” refers to the maximum number of molecules of X per cell (only relevant for molecular species that undergo explicit stoichiometric reactions such as hetero-dimerization); and the subscripts “Endo” and “Exo” refer to endo- and exo-cytosis, respectively, whereas “LMxfer” and “Mxfer” refer to exchange between adjacent and apposite cell faces, respectively. Ranges are discussed in the Supplement to von Dassow et al. (2000), but briefly, half-maximal coefficients, flux rates, transformation rates, and most other parameters range over 3 orders of magnitude on a log scale. All half-maximal coefficients range from  $10^{-3}$  to 1.0, where all concentrations are normalized to the maximal possible steady-state level for the relevant molecular species. Half-lives range linearly from 5 to 100 min, cooperativity coefficients range linearly from 2.0 to 10.0 (except  $v_{PTC-CID}$ ), and saturability coefficients range linearly from 1.0 to 10.0. These histograms result from a search of 235,875 randomly chosen parameter sets from within those ranges, in which 1,120 “working” sets were found. In several identical searches, the biases shown here are reproducible, but for the most part the small wiggles are not.



N-terminal repressor form of the Cubitus interruptus protein is an avid repressor of *wingless* transcription. These observations of the model may correspond to empirical evidence. In particular, in *ptc<sup>-</sup>;wg<sup>ts</sup>* embryos, Wg cannot contribute to its own expression, but Ci presumably remains uncleaved in the absence of Ptc; only weak *wg* expression is observed in these embryos, showing that full-length Ci by itself is a poor activator of *wg* (Hooper, '94). Also, Von Ohlen and colleagues showed that, in cultured cells, Ci is a weak activator of the large *wg* enhancer fragments, although it strengthens substantially when smaller pieces concentrating candidate Ci binding sites are used as the test substrate (Von Ohlen and Hooper, '97; Von Ohlen et al., '97). Their findings suggest that other, perhaps generic, factors limit the effectiveness of Ci in the context of the full *wingless* transcription unit.

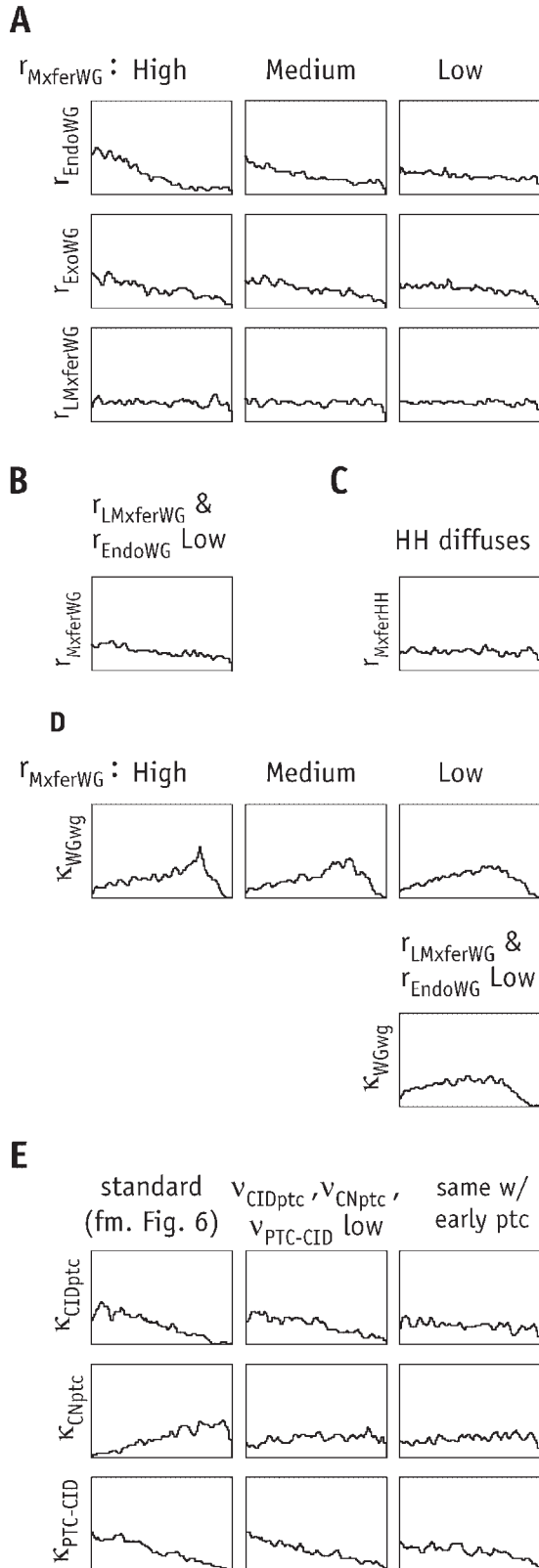
Other parallels are evident between our model's parameter preferences and the available empirical evidence. For instance, the core model prefers that Engrailed not be too good a repressor of *cubitus interruptus* transcription (Fig. 6, column 1, row 9). At the compartment boundary in imaginal discs, *en* is expressed in anterior compartment cells closest to the boundary, but does no more than slightly diminish the expression of *ci* in those cells (Strigini and Cohen, '97). In contrast, our core model does *not* appear to correspond to empirical observations on another target of Ci, *patched* (Fig. 6, column 1, rows 6 and 7). The model prefers Ci to be a good activator but CN a weak repressor of *ptc*. Holmgren and colleagues have shown that near the anterior-posterior compartment boundary in wing imaginal discs, while *decapentaplegic* transcription is activated at relatively low levels of Hh signaling, i.e., at a low ratio of full-length Ci to the repressor form, *ptc* is activated only at much higher levels of Hh signaling and thus higher ratios of Ci to CN (Wang and Holmgren, '99). These authors even propose that Ci must be hyper-activated at the highest levels of Hh signaling in order to activate *ptc*. We explore some possible reasons for this discrepancy shortly.

Interestingly, the model prefers low rates of Wg transport (Fig. 6, column 5, rows 3–5). Among the most striking biases in Figure 6 is toward low values for the rate of cell-to-cell Wg exchange (row 5). For many years it was disputed whether Wg ever diffused at all from the cells in which it is synthesized (for example see Gonzalez et al., '91; Vincent and Lawrence, '94; for review see Martinez-Arias, '93). Although the evidence has re-

cently become fairly conclusive that Wg protein does indeed travel a considerable distance from its site of synthesis, there is still much debate about how it does so (i.e., by free diffusion or transcytosis) and in what form (free or bound to its receptors or other proteins), or even if Wg is carried by cells migrating within the plane of the epithelium (Hacker et al., '97; Cadigan et al., '98; Dierick and Bejsovec, '98; Moline et al., '99; Pfeiffer and Vincent, '99; Sanson et al., '99; The and Perrimon, 2000; Strigini and Cohen, 2000). We permitted Wg to be endocytosed and then re-exocytosed in our models to allow for the possibility of transcytosis, so the core model subsumes transcytosis, "free" diffusion, and other mechanisms.

We wondered if Wg transport rates constrain other parameters in the model. To test this we constrained the Wg "diffusion" rate  $r_{\text{MxferWg}}$  (really a cell-surface-to-apposite-cell-surface exchange reaction rate) to vary only within high, medium, and low sub-ranges and then assessed the resulting frequency of solutions in a random sample of parameter sets (Meir et al., 2002b). Solutions are roughly three times more frequent when Wg diffusion is slow (with a half-time for equilibration on the order of hours) compared to when it is fast (half-time on the order of minutes).<sup>2</sup> The distributions of all other Wg transport rates showed strong responses to the imposed constraint: if Wg "diffusion" is rapid, then all these other rates are constrained to be slow, whereas if Wg diffusion is slow, then these other parameters exhibit flat distributions (Fig. 7A). The converse is also true: if transcytosis of Wg via endocytosis, re-exocytosis, and transport within the cell membrane is slowed by constraining the appropriate rates ( $r_{\text{EndoWg}}$  and  $r_{\text{LMxferWg}}$ ), the constraint upon Wg cell-to-cell transport is largely alleviated (Fig. 7B). The only other parameter for which we detected sensitivity to Wg transport rates was the half-maximal coefficient governing Wg auto-regulation. In an unconstrained random sampling, this parameter ( $\kappa_{\text{WGwg}}$ ) is distributed in a broad, gentle hump centered around values for which Wg is a moderately weak activator of its own

<sup>2</sup>The actual parameter used is a dimensionless product of a first-order rate constant and the characteristic time constant (usually 1 min). The reaction in question is a concentration-dependent exchange between one cell face and the apposite face of the neighboring cell, in the case of cell-to-cell "diffusion," or between one cell face and the adjacent face of the same cell, in the case of "diffusion" within the membrane of an individual cell. The inverse of the first-order rate constant, the time constant, or its relative the half-time, is easier to express in words. When the rate constant is large, the reaction is fast and the half-time small, and vice versa.



production (Fig. 6). If Wg is allowed to diffuse rapidly, this hump sharpens into a rather abrupt peak, although there remain solutions for most portions of the entire range; if Wg diffusion is slow, the hump erodes (Fig. 7D). It likewise erodes when we prevent transcytosis.

Originally we omitted cell-to-cell Hh transport. Hh is synthesized as a transmembrane protein but is autolytically processed (Porter et al., 1996a,b) to a cholesterol-tethered form. Processed Hh, at least in some tissues, travels quite far from its site of synthesis (Strigini and Cohen, '97), but it may require assistance from other proteins to do so (Bellaiche et al., '98; Burke et al., '99). However, there is almost no detectable negative effect of Hh cell-to-cell transport when we introduce it to the model. In fact, this process had a very slight but reproducible *positive* effect on the frequency of solutions (see Meir et al., unpublished observations), but independent of the actual rate of the process: the distribution of the Hh diffusion rate is flat (Fig. 7C).

Thus the model exhibits subtle constraints and trade-offs with regard to parameter distributions, many of which correspond to empirical observations. On the basis of the results described in Figure 6 and other results not shown, we tried to identify a sub-region of the parameter space in which solutions are most frequent. By trial and error we came up with the region described in Table 1. In this region, the ranges of the half-maximal coefficients were restricted to the 10-fold range that best matched the peaks in Figure 6. Most cooperativity coefficients were forced to be fairly high except (following the results reported in Meir et al., 2002b) those governing interactions between *ptc* and *ci*, which were allowed their full ranges. All half-lives remained unconstrained,

←

Fig. 7. Parameter distributions as a function of parameter constraints. Histograms as in Fig. 6. For panels **A–D**, the searches are documented in the companion paper by Meir et al. (2002b, this issue); for panel **E** the results are cited in the text. (**A**) High rates of Wg cell-to-cell diffusion (governed by the parameter  $r_{MxferWG}$ ) impose a leftward bias on other Wg transport rates; slow Wg diffusion rates ameliorate this effect. (**B**) Constraining Wg endocytosis and intra-membrane diffusion to low rates alleviates the bias on Wg cell-to-cell diffusion. (**C**) There is no bias on the rate of Hh cell-to-cell diffusion. (**D**) Subtle influence of Wg cell-to-cell diffusion on *wg* autoregulation. (**E**) Lowering cooperativity of *ptc-ci* interactions, and providing ubiquitous early *ptc*, alleviate constraints on half-maximal coefficients governing Ci/CN regulation of *ptc*. Left column of panel **E** is taken from Fig. 6 to facilitate direct comparison.

TABLE 1. Canyon in parameter space, inferred from distribution of hits in the standard box<sup>1</sup>

Parameter	Qualitative interpretation	Constraint	Bounds
$\kappa_{WGen}$	WG activation of <i>en</i>	Moderate	0.01–0.1
$\kappa_{CNen}$	CN repression of <i>en</i>	Strong	0.002–0.02
$\kappa_{WGwg}$	WG autoactivation	Moderate	0.01–0.1
$\kappa_{CIDwg}$	CID activation of <i>wg</i>	Weak	0.2–2.0
$\kappa_{CNwg}$	CN repression of <i>wg</i>	Strong	0.002–0.02
$\kappa_{CIDptc}$	CID activation of <i>ptc</i>	Strong	0.002–0.02
$\kappa_{CNptc}$	CN repression of <i>ptc</i>	Weak	0.1–1.0
$\kappa_{ENcid}$	EN repression of <i>cid</i>	Moderate	0.02–0.2
$\kappa_{PTCCID}$	PTC stimulation of CID cleavage	Strong	0.002–0.02
$\kappa_{ENhh}$	EN activation of <i>hh</i>	Weak	0.1–1.0
$\kappa_{CNhh}$	CN repression of <i>hh</i>	Strong	0.002–0.02
$C_{CID}$	Max. cleavage rate of CID	Rapid	0.1–1.0
$v$ (e.g., $v_{CIDptc}$ , $v_{CNptc}$ , $v_{PTCCID}$ )	Cooperativity coefficients	Steep	5.0–10.0
$H_{IWG}$	Half-life of intracellular WG	Short	5.0–30.0 min.
$r_{EndoWG}$	Rate of WG endocytosis	Slow	0.001–0.01
$r_{ExoWG}$	Rate of WG exocytosis	Moderately slow	0.005–0.05
$r_{MxferWG}$	Rate of WG cell-to-cell exchange	Slow	0.002–0.02

<sup>1</sup>Within the canyon described by the constraints tabulated below, we obtained 1,017 hits in 1,284 random parameter picks, a hit rate of 4 out of 5 (1 in 1.26), with an average score of 0.060 (substantially better than the standard box average score of 0.077; the best score possible is approximately 0.035, the cutoff above which patterns are rejected is 0.2).

except for the half-life of the intracellular form of Wg, which we constrained to be low. Finally, rates governing Wg transport were constrained to be low. Within this region, the frequency of solutions is an astounding 4 out of 5 randomly chosen sets. Thus, Table 1 describes a vast, steep-sided canyon in the “epigenetic landscape” for the model, within which the model is almost completely insensitive to the exact value chosen for any parameter, and in which mutual constraints among parameters all but disappear. Most strikingly, the constraints that define this Grand Canyon are very similar, except for the issue of *ptc* regulation (see below), to what we would have come up with had we guessed from the available empirical data.

### The *ci*–*ptc* negative feedback loop

It bothered us that the model should seem to prefer *Ci* to be an avid activator of *ptc* when empirical evidence suggests the opposite (see above). Furthermore, we had long been puzzled by a persistent defect in the time-varying behavior of the core network: it seems very difficult to achieve stable patterns of expression for either *Ci* protein forms or for *ptc*. For many parameter sets that gave stable *en*, *wg*, and *hh* expression patterns, the *Ci* protein levels oscillated in time.<sup>3</sup>

<sup>3</sup>“Stable” versus “oscillatory” is a matter of degree. Nature surely does not know the difference between a true stable steady state point and a small-amplitude limit cycle. However, we assume that large-

These defects do not prevent the model from mimicking the patterns of *wg*, *en*, and *hh*, which are the primary regulators of downstream processes like cuticle patterning and neurogenesis.

We noticed that when individual cooperativity coefficients are held fixed at 1.0 (non-cooperative), for three parameters the solution frequency actually increases slightly (see companion paper by Meir et al., 2002b, this issue). Those three govern direct links between *Ci* and *ptc*. We thus restricted these three cooperativity coefficients to vary only between 1.0 and 2.0, thus allowing only very mild cooperativity in these links, and re-ran the random sample. We obtained 1,200 solutions in 126,525 samples (1 in 105), a significant improvement. In addition, this restriction slightly ameliorated the bias on repression of *ptc* by CN (Fig. 7E). Almost all the solutions found conferred stable expression patterns on *Ci* and CN and *ptc*, and many exhibited the canonical pattern of *Ci* versus CN distribution (high *Ci* next to Hh-producing cells, high CN elsewhere) and of *ptc* (stripes next to the Hh-producing cells). Although in the companion paper (Meir et al., 2002b, this issue) we showed that the global level of cooperativity is positively correlated with robustness of the model, clearly these results demonstrate that

amplitude oscillations or chaotic behavior are functionally very different from small limit cycles in many developmental contexts. Our scoring functions take these considerations into account.

TABLE 2. Sensitivity of the core network to gene dose<sup>1</sup>

Locus	Heterozygote	1 extra copy	2 extra copies	4 extra copies	6 extra copies
En	628 (56%)	872 (78%)	706 (63%)	516 (46%)	361 (32%)
Ci	678 (60%)	1,027 (92%)	968 (86%)	886 (79%)	841 (75%)
Ptc	901 (80%)	1,104 (99%)	1,101 (98%)	1,098 (98%)	1,091 (97%)
Hh	379 (34%)	1,064 (95%)	1,029 (92%)	964 (86%)	872 (78%)
Wg	339 (30%)	806 (72%)	646 (58%)	449 (40%)	333 (30%)

<sup>1</sup>The fraction of the 1,120 good parameter sets (same sets in Fig. 6 and the top line of Table 3 in the companion paper by Meir et al. (2002b, this issue) which also make the right pattern in the presence of different copy numbers for constituent genes. Percents are given in parentheses.

cooperativity in regulatory interactions does not in every case foster robustness.

There remained a noticeable bias favoring strong activation of *ptc* by full-length Ci. We show below that the solution frequency increases when we include initial ubiquitous, moderate expression of *ptc* in the prepattern. CN repression of *en* is crucial; starting with our standard initial conditions, *ci* and *en* race for control of the cell state. Perhaps Ci must be a strong activator of *ptc* only so as to quickly get itself converted into a repressor and squelch the spread of Wg-stimulated *en* expression. We thus conducted another sampling with the same constraints on Ci-*ptc*-related cooperativity coefficients and with initial ubiquitous expression of *ptc* mRNA and protein in the prepattern, and found 1,127 in 68,114 solutions (1 in 60). The bias on both Ci activation of *ptc* and on CN inhibition of *ptc* all but disappeared (Fig. 7E).<sup>4</sup>

### Sensitivity to gene dose

Uncoordinated variations in single parameters are a good proxy for a subset of likely mutations that one would expect to afflict real genes. For instance, a particular mutation might modify a single nucleotide in the enhancer of some gene X, allowing it to bind with lowered affinity to some essential activator Y; this would be analogous to an increase in the parameter  $\kappa_{YX}$  in our modeling formulation. However, many mutations will likely lead to predictably coordinated changes in several parameters at once. A simple way to impose

coordinated changes in the parameters for each gene is to vary the copy number. We tested what fraction of solutions succeed as heterozygotes or with 1, 2, 4, or 6 additional copies of each locus individually (Table 2). Notably, for the core model most solutions are almost completely insensitive to extra copies of *ptc*, *hh*, and *ci*. The model seems rather more sensitive to heterozygosity for *hh* and to dosage variation in either direction for *wg* and *en*. However, this is simply because the goodness-of-fit function that scores the behavior of the model (see Supplementary Information for von Dassow et al., 2000) is moderately sensitive to the quantitative level of expression of the species it monitors. We watched the entire test suite for *hh* and *wg* heterozygotes, and observed that most of the parameter sets that fail do so only because the reduced gene dose, of course, reduces proportionally the maximal level to which the gene's products accumulate. In most cases the *wg*- or *hh*-heterozygous model makes a qualitatively correct pattern which fails merely because some of the concentrations are too low to pass the goodness-of-fit cutoff. For *wg* heterozygotes, roughly 75% would have passed had we relaxed the stringency of the scoring function accordingly; for *hh* heterozygotes, all but a few would have passed.

Nevertheless, we stick with the more stringent measure, because from the perspective of the segment polarity network's downstream targets the absolute level of segment polarity gene expression could be important. Even so, many parameter sets tolerate quite a lot of variation in gene dose: 61 out of 1,120 solutions tolerated heterozygosity at all loci, and of those 61, the vast majority (56) also tolerated an extra copy of every locus. If these were uncorrelated responses, then on the basis of Table 2 one would expect only about 1% of the 1,120 to survive both heterozygosity for and an extra copy of all loci; the fact that 5% survived suggests that these are an

<sup>4</sup>This latter observation is unlikely to be relevant to *Drosophila* development, because pair-rule gene products persist on the order of an hour after segment polarity genes first come to be expressed, and provide a temporary, fading influence that guides the early sorting out of intrasegmental cell states (Martinez-Arias, '93). We have explored how they do so in the context of this model and their influence on robustness (which is generally positive), but do not report these results here. It is, however, unknown how the segment polarity genes acquire their initial patterns in other arthropods. Especially in short-germ insect embryos, the segment polarity module may not be able to count on pair-rule genes for guidance.

especially robust subset. Of those, 12 parameter sets tolerated all tested gene dose variations. This shows, on the one hand, that it is possible to find parameters that make the network robust to 12-fold variation in the dose of every locus. However, those 12 sets came from a search of 235,000 random samples, so their frequency is about 1 in  $2 \times 10^4$ . While this is still a high frequency (see the hypothetical comparison in von Dassow et al., 2000, to an engineered circuit), the fact that only a fraction of solutions tolerate heterozygosity suggests an evolutionary rationale for robustness. While it is hard to imagine that organisms experience significant selection to tolerate heterozygosity or extra copies of genes, certain other phenomena, from the point of view of the gene network, seem very similar. For example, embryos differ significantly in volume and can be induced to differ even more in response to extreme conditions (our unpublished observations). Cells probably differ stochastically in the availability of biosynthetic machinery, or time spent in interphase, or many other factors. Selection for robustness against such non-heritable variation would likely render the network robust to genetic variation that alters gene expression levels.

## Summary

In this section we showed that the parameter space of the core segment polarity model embodies various constraints on individual parameters, including trade-offs among several parameters controlling a particular kinetic process. These constraints reveal a sub-region of the parameter space, still vast, in which the model is almost guaranteed to work. We suggest the visual metaphor of Grand Canyon, with smaller tributaries (within which the model works, but not as robustly) snaking in from the surrounding plateaus to join a wide, steep-walled main canal.

### Section II: Architectural variants of the core network model

The core network model lacks certain known or suspected interactions among its components. An example is that En is claimed to repress *ptc* (Sanicola et al., '95), although it is not clear whether this interaction is direct or mediated through En repression of *ci*. In addition, since we could not see why this interaction should be necessary for the function of the network, we initially chose to leave it out. Again, our goal is to reconstitute, not make a complete re-creation a

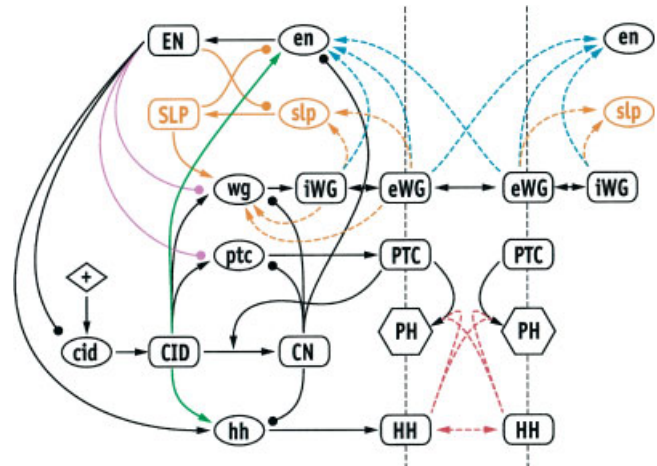


Fig. 8. Architectural variants of the core network. The entire network inhabits each cell; also diagrammed for clarity are the direct effects of one cell on its neighbor (WG=wingless, EN=engrailed, SLP=sloppy paired, HH=hedgehog, CID=cubitus interruptus (whole protein), CN=repressor fragment of cubitus interruptus, PTC=patched, PH=Patched-Hedgehog complex). Ellipses represent mRNAs; rectangles, proteins; and hexagons, protein complexes. Arrows represent positive interactions; round-ended lines, negative ones. Solid black lines represent interactions that remain in place in all variants. Colored lines indicate the variants documented in Table 3. Dashed lines indicate mutually exclusive choices; no two dashed lines of the same color exist in any one model.

priori. The core network model also embodies certain assumptions about the specific nature of the interactions among its components. For instance, *wg* autoregulation is mediated by the intracellular, rather than the extracellular form of the Wg protein (this seemingly bizarre choice was supported by empirical observations reported by others; see below). We next test the extent to which these choices affect the performance of the network. Figure 8 diagrams the core network and the variants to be explored in this section. Colored lines indicate additional links; dashed lines indicate alternative choices, and no variant embodies two dashed lines of the same color. Table 3 describes these variants and the results of random samplings conducted as above.

### Repression of patched by Engrailed

Introduction of a link by which En represses *ptc* slightly decreased the frequency of solutions. However, any such addition increases the dimension of parameter space. Any bias on the distribution of these novel parameters, as for several

TABLE 3. Architectural variants of the core network, and their consequences<sup>†</sup>

Original topology (reference for spgl)	1120	235,875	1 in 211
Variant: what if...	No. of hits	No. of tries	Hit rate
1 EN represses ptc transcription	344	107,574	1 in 313
2 EN represses ptc, plus ubiquitous initial ptc	724	101,175	1 in 140
3 Ubiquitous early ptc expression	896	97,339	1 in 109
4 CI activates en	730	260,943	1 in 357
5 CI activates hh	680	260,142	1 in 383
6 Ci/CN-en/hh			
Var. A: CI activates hh & en, CN a global repressor of both en and hh	198	122,401	1 in 618
Var. B: CN a competitive inhibitor of CI w.r.t. hh regulation (i.e. local hh inhibitor)	69	120,861	1 in 1,751
Var. C: CN a global hh repressor, but a local inhibitor of en: Ci/CN synergizes w/Wg in en activation	5	121,1235	1 in > 10 <sup>4</sup>
Var. D: C but with CN a local hh inhibitor	4	117,626	1 in > 10 <sup>4</sup>
10 EN represses wg transcription	538	237,764	1 in 442
11 eWG on cell's surface (instead of neighbors) activates en transcription	486	190,661	1 in 392
12 iWG, not eWG, activates en transcription	171	196,669	1 in 1,150
13 eWG, not iWG, mediates wg autoregulation	456	189,824	1 in 416
14 Slp Var. A: eWG activates slp transcription, en regulation like line 11 above	347	163,784	1 in 472
15 Slp Var. A with initial slp stripe in wg row	839	153,495	1 in 183
16 Slp Var. B: iWG activates slp transcription, en regulation like line 11 above	775	160,882	1 in 208
17 Slp Var. B plus initial slp stripe in wg row	1538	143,798	1 in 93
18 Slp Var. C: same as B but iWG activates en (like line 12 above)	281	161,840	1 in 576
19 Slp Var. C plus initial slp stripe in wg row	751	158,856	1 in 212
20 Slp Var. D: A but with en regulation as in original model	533	152,351	1 in 286
21 Slp Var. D plus initial slp stripe in wg row	1021	141,805	1 in 139
22 Slp Var. E: B but with en regulation as in original model	1032	147,460	1 in 143
23 Slp Var. E plus initial slp stripe in wg row	1595	135,036	1 in 85

<sup>†</sup>Top line (reference model) is the same data as Table 3 in the companion paper by Meir et al. (2002b, this issue). Parameter ranges as described in Figure 6; spgl variants are diagrammed in Figure 8.

of the original parameters, will cause a decrease in the frequency in the absence of constraints. Thus the effect of adding the *En-ptc* link was unremarkable. We wondered, however, why such a link might exist. Although in our standard tests the initial conditions consist only of stripes of *wg* and *en* and the corresponding proteins, in reality the prepatterning confronted by the segment polarity network in a blastoderm-stage *Drosophila* embryo is much more complex. In particular, *ptc* is expressed nearly ubiquitously until mid-germ band extension, disappearing from *en*-expressing cells by stage 9, and finally coming to be expressed only on each side of the *en*-expressing stripe at stage 11 (Hooper and Scott, '89). Indeed, in the context of initial background levels of *ptc*, the *En-ptc* link increases the solution frequency. However, even in the absence of the *En-ptc* link the frequency of solutions increased when the initial conditions included a moderate background level of *ptc*. We suspect this is because Ptc promotes conversion of basally expressed Ci into the repressor, CN, which then prevents *en* expression from spreading beyond its initial stripe.

### Potential targets of Cubitus interruptus

The core network includes one link whose reality is questionable: the repression of *en* by CN. We justified this link (von Dassow et al., 2000) on the basis of two published observations: (1) antibodies to Ci stain the polytene chromosome band in which the *engrailed* gene resides (Aza-Blanc et al., '97), and (2) *smoothed*-dependent Hh signaling activates *en* expression just anterior to the compartment boundary in imaginal discs (Blair and Ralston, '97; Strigini and Cohen, '97) and abdominal epidermis (Lawrence et al., '99), presumably through the known Smo signaling pathway that terminates in the regulation of Ci cleavage. Since other known positive targets of the full-length Ci protein are repressed by the N-terminal fragment, we felt justified in hypothesizing the *CN-en* link. Why not then include a *positive* link between full-length Ci and *en*? When we do so, the frequency of solutions drops. This merely says that if such a positive link exists, it must be a weak one, and on the basis of the narrow stripe of imaginal disc cells in which *en* is activated by Hh signaling, this must be the case. By analogous reasoning, since in our model CN represses *hh*, should not Ci activate *hh*? As with *en*, if it does so the model suffers slightly, but only

to the extent that this added interaction must not be too strong.<sup>5</sup>

Even if full-length Ci does not actually regulate either *en* or *hh* in the early embryo, *then surely these links are near-neighbors in the space of possible evolutionary changes*, since Ci and CN have the same DNA binding domain. CN probably acts as a repressor by competing with full-length Ci for binding to consensus sites, and thus ought to be a local repressor of transcription. However, in the context of our model we had to assume that CN is a global repressor of *en* and *hh*. CN could accomplish this if some factor recruited by full-length Ci (CBP perhaps?) is required for transcription of these targets. We tried several different ways of hooking up these links, including models in which CN is a global repressor of both *en* and *hh*, or of one or the other, or of neither. Table 3 includes the results from several of these, and shows that these choices can be very important to the performance of the model; if indeed these links are easy to establish, then the network is in a dangerous evolutionary neighborhood with respect to this part of the circuit.

### Wingless transport

In our core model we chose to make *en* sensitive to the concentration of Wg on apposite cell surfaces; that is, cells respond to Wg protein presented to them by their neighbors. We tested whether it makes any difference to the model if Wg must first become associated with the responding cell's surface (Table 3). The modest penalty shown in Table 3 (line 11 versus top line) likely results from the fact that in order for this transfer to take place the Wg diffusion rate, which the model prefers to be slow, must be sufficient to get the protein from the cell in which it is synthesized to the cell in which it is sensed. This result underscores the suggestion that control of Wg traffic is likely to be a critical parameter for optimizing the most basic functions of the segment polarity network. We next tested whether it makes any difference (to the model) whether *wg* autoregulation is mediated by intracellular or extracellular Wg protein. As shown in Table 3, line 13, the frequency is lower for a model in which extracellular Wg stimulates *wg* transcription.

<sup>5</sup>It should be noted first that we are aware of no evidence for positive regulation of *hh* by Ci. Indeed, the only evidence available is that *some* product of *ci* must repress *hh* (Dominguez et al., '96), and we merely assumed it is the N-terminal fragment. Full-length Ci binds to (and requires) the co-activator CBP to activate its targets (Akimaru et al., '97; Chen et al., 2000). In some contexts CBP behaves as a co-repressor (Waltzer and Bienz, '98), so it is possible that full-length Ci is responsible for *hh* (and even conceivably *en*) repression.

Our choice of intracellular Wg for this role is supported by the analysis of certain *wg* alleles in which abundant Wg protein remains localized to the cell in which it is synthesized. These alleles block maintenance of *en* expression by Wg, but not *wg* autoregulation (Dierick and Bejsovec, '98). However, Hooper ('94) showed that the *wg* autoregulation mechanism is able to spread from cell to cell in the segment, and Manoukian et al. ('95) showed that *porcupine*, a membrane protein involved in Wg glycosylation and secretion (Tanaka et al., 2002), is required for *wg* autoregulation. The observations of Hooper and Manoukian might be reconciled with those of Dierick and Bejsovec by assuming that Wg moves among cells by transcytosis. Our model shows these hypotheses are dynamically plausible, but clearly we need more detailed experimental information on Wg transport and the autoregulatory pathway.

### **Sloppy-paired as a candidate intermediate for wingless autoregulation**

We considered two candidates for intermediate steps in *wg* autoregulation. First, several pieces of suggestive evidence implicate the protein kinase encoded by *fused* in this process (Hooper, '94; Therond et al., '99). The Fu kinase phosphorylates Ci, and perhaps this phosphorylation could hyperactivate Ci (Ohlmeyer and Kalderon, '98); if in addition Fu activity is somehow stimulated by Wg signaling, this could account for *wg* autoregulation. So far, however, we have failed to incorporate a complete, self-consistent set of hypotheses about how the action of *fused* and other components of the Hh signal transduction pathway could mediate *wg* autoregulation.

A better candidate is the transcription factor encoded by *sloppy-paired*. Slp activates *wg* and represses *en* (Cadigan et al., 1994a,b). In addition, recent reports suggest that *slp* is itself activated by Wg signaling and repressed by En (Kobayashi et al., '98; Bhat et al., 2000; Lee and Frasch, 2000). *slp* is expressed in the Wg-producing cells and their immediate neighbors to the anterior and therefore is an excellent candidate for an intermediate in *wg* autoregulation (see Fig. 8), although from published reports it is not clear for how long *slp* is expressed in embryogenesis. As shown in Table 3, models in which *wg* is autocatalytic only via *slp* perform admirably.

We noticed while watching the random sampling process work over models using *slp* to mediate *wg* autoregulation that many parameter

sets failed because Wg expression declined before *slp* expression ramped up. *slp* is actually expressed substantially earlier than the other segment polarity genes (Grossniklaus et al., '92). When we include an initial stripe of *slp* mRNA and protein in the prepatter (an entirely legitimate element in flies but unknown for other insects) the hit rate improves for obvious reasons. The initial *slp* stripe also made the model less sensitive to certain details, such as which compartmental form of Wg activates *en*. This is because the initial *slp* stripe keeps *en* from invading the *wg* row.<sup>6</sup>

### **Summary**

The robustness of the segment polarity model is not due to particular ad hoc wiring choices. Rather, our attempt at a reconstitution resulted in a robust core topology, and that core model is robust not only to variation in parameters and initial conditions (von Dassow et al., 2000) but also to variation in the architecture of the network, so long as the architectural variants use realistic connections. We have tested numerous realistic possibilities that can be addressed *within the context of the simple model of the core segment polarity network, and with respect to its basic boundary-maintaining function*. Most of the variants we tested have only subtle impacts on the performance of the model, but Table 3 shows that clearly one *can* introduce connections that impose major constraints. Before leaving the simple model, we emphasize that the map in Figure 8 encompasses facts known with varying degrees of confidence. In the process of concocting a model of any biological process, gene network behavior in this case, one confronts unknowns in which some decision must be made in the absence of adequate evidence. The modeling approach used here and described in the companion paper (Meir et al., 2002b, this issue), which relies on a stereotyped set of building blocks to express gene regulatory interactions, allows us to rapidly test the plausibility and mutual consistency of hypothetical mechanisms and quickly compare models embodying different choices.

### **Section III: Maps at lower and higher resolution**

The segment polarity model seeks to express in mathematics certain kinetic processes described

<sup>6</sup>See the companion paper by Meir et al. (2002b, this issue) for demonstration that, under relatively tightly specified conditions, a sub-network consisting of just *slp*, *wg*, and *en* can do the same job as the whole network, but not robustly.



by biologists. To what extent do the results depend on the level of detail incorporated in the model? Overly simplistic models fail to incorporate mechanistic constraints that Nature faces. For example, the core segment polarity model expresses mathematically the English statement “Wingless activates *engrailed* transcription”, but Nature has to design a signaling pathway by which it does so, and the chosen design may have important consequences to the robustness of the mechanism as a whole. On the other hand, too complex a model becomes useless as an explanatory tool. In this section we compare models of lesser or greater complexity.

### Simpler versions

First, we tested a simplified model that is topologically identical to the core network but collapses the mRNA and protein products of every locus into a single entity. The collapsed model has slightly fewer parameters but, again, *exactly the same topology*. We found that it is quite capable of making the desired pattern, but solutions are five times less frequent: the hit rate in a random sample was roughly 1 in 1,000. Furthermore, somewhat contrary to our naïve expectations, the collapsed model is computationally *less* tractable: it takes about an order of magnitude more computer effort *per parameter set* to integrate the collapsed model in searches equivalent to those performed with the core model.

Both the lowered solution frequency and the increased stiffness of the equations are due to the fact that the collapsed model is much more prone to large-amplitude temporal oscillations than is the core model. Collapsing the mRNA and protein into a single species eliminates a major source of kinetic delays (e.g., when an mRNA declines temporarily, the protein declines a little later). While delays are generally thought of as a *source* of oscillations, in this case the existence of an intermediate step between stimulus (input into a gene’s enhancer region) and response (accumulation of the protein product to equilibrium level) tends to damp out oscillations. The desired behavior for the segment polarity model is based on positively reinforcing but mutually exclusive stable cell states. A balance of positive feedback and negative crosstalk promotes this behavior. The model includes at least one prominent negative feedback loop (between Ptc and Ci) that tends to generate oscillations. Whether or not these oscillations propagate to the positive feed-

back loops that stabilize cell states depends both on the relative time scale with which each component responds and also on how well non-linear thresholds buffer each component from oscillations in input stimuli. In the core model, all transcriptional responses involve ramping up or down the level of two different species which could have very different half-lives. Since the half-lives determine how long it takes each species to reach equilibrium, the response to an oscillatory input is damped by the slowest-equilibrating step in the chain. In contrast, in the collapsed model, there are half as many opportunities to damp oscillations, and thus a much greater fraction of the parameter space succumbs to oscillations that probably originate in the Ci/Ptc negative feedback loop. It is not yet clear to us whether this finding is specific to this particular network, but it is possible that gene networks are “designed” to exploit dynamical rules like these to stabilize gene expression levels.

Second, we attempted to concoct a different and much simpler “engineered” model that would accomplish the same task of stabilizing two different cell states right next to one another. After many failures, we accomplished this using two loci encoding diffusible proteins, each of which somehow activates itself, suppresses the other, and hetero-dimerizes with the other to form a substance that activates expression of both genes (Fig. 9A). This toy model can work but is far less robust to parameter variation than is the segment polarity network model (Fig. 9B). With 27 free parameters, the solution frequency was on the order of  $<1$  in  $10^4$  ( $n=29$  hits). If the kinetics of the two loci’s products are constrained to be symmetric (e.g., if A and B have identical half-lives, diffusion coefficients, avidity for targets, etc.), then the solution frequency becomes more amenable (1 in  $\approx 150$ ,  $n=646$  hits, 16 free parameters), but this is a very stringent constraint! If the mRNAs and proteins are collapsed into single nodes as above, this design breaks down completely; there must exist some scarce solution somewhere in the parameter space of the collapsed version, but we have not yet discovered its hiding place, even with hand tuning.<sup>7</sup> Perhaps we are just poor engineers, and some other elegant

<sup>7</sup>The reason is essentially the same as in the collapsed model of the segment polarity network: cut out the intermediate steps, and the model becomes much more susceptible to oscillations driven by negative feedback. Thus our experience with the engineered toy substantiates our explanation for the segment polarity network, and hints at the possibility of a general rule for designing robust genetic mechanisms.

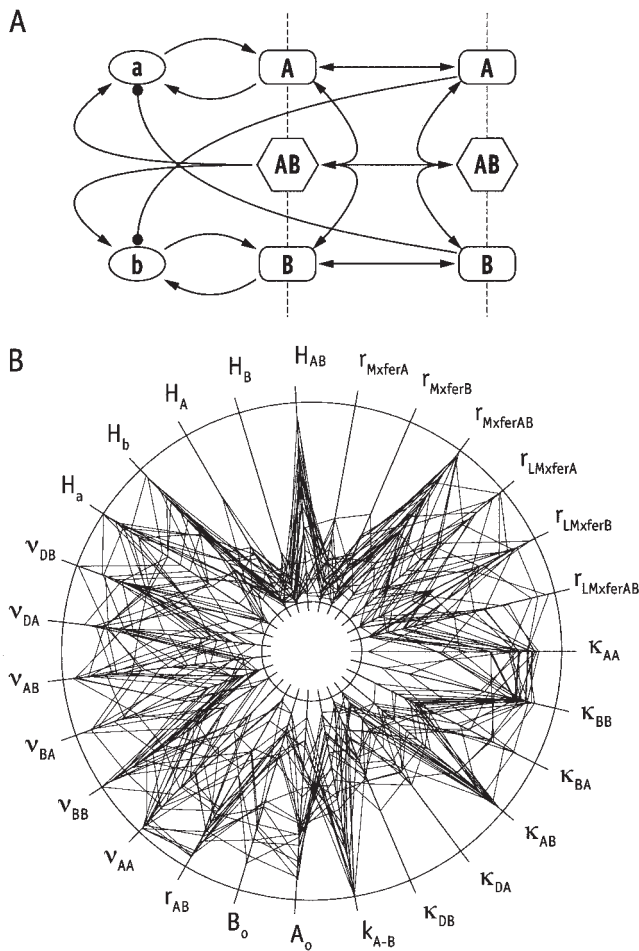


Fig. 9. Simple network that does a similar task to the segment polarity network. (A) Topology of the concocted network; A and B are secreted proteins that promote their own expression but repress each other; they dimerize to produce a diffusible complex which functions as an activator of both loci. (B) Wheel plot of parameter sets that succeed in holding a boundary with an A-expressing cell state to the anterior and a B-expressing cell state to the posterior. Clearly there are sharp biases on certain parameters. Not apparent is the strong preference for A and B to be symmetric, i.e., to be governed by nearly identical values for every parameter (see main text).

device might do better. However, it is *not* the case that the network in Figure 9A represents an intrinsically poor design; we managed, indeed, to build it up until it became quite robust, at which point it had concomitantly grown almost as complex as the core segment polarity network (not shown).

A third simplification is discussed in the companion paper by Meir et al. (2002b, this issue). We found that a sub-network consisting of *wg*, *en*, and *slp* is capable of accomplishing the same

boundary-maintenance task as the core segment polarity network, but it is not nearly as robust to initial conditions or to parameter variation. Thus the core segment polarity model is not, as we originally reported (von Dassow et al., 2000), the simplest realistic topology capable of accomplishing this task; rather, adding another component, *slp*, allows one to break the network into two pieces, one of which can do the basic task required, but which becomes more robust when coupled to the other sub-network.

### Incorporating a signal transduction pathway for Wg

The core model omits the dynamics of the signal transduction pathway between Wg and *en*. A brief summary of the real pathway would begin with secretion of Wg from cells that synthesize it. Once secreted, Wg interacts with a number of cell surface proteins, including receptors in the Frizzled family (Bhanot et al., '96, '99; Bhat, '98; Sato et al., '99; Sivasankaran et al., 2000), the transmembrane receptor Notch (Wesley, '99), and heparan sulfate proteoglycans (Hacker et al., '97; Lin and Perrimon, '99; Tsuda et al., '99). We are not aware of any role for Notch in segment boundary maintenance in the early embryo. Heparan sulfate proteoglycans may restrict Wg traffic across the parasegment boundary, but this role may or may not affect segment boundary maintenance. The products of three related genes, *frizzled* (*fz*), *Dfrizzled2* (*Dfz2*), and *Dfrizzled3* (*Dfz3*) are the receptors involved in *en* regulation by Wg. *fz* was originally discovered as a tissue polarity gene (Vinson et al., '89), and it seemingly retains a sociological association with that function. *Dfz3* exhibits little signaling activity and may serve primarily as an attenuator of Wg signaling (Sato et al., '99). Thus *Dfz2* assumes the mantle of "the Wingless receptor." Nevertheless all three are expressed in early fly embryos, and at least *fz* and *Dfz2* can substitute for one another during segmentation (Bhanot et al., '99; Chen and Struhl, '99). Hereafter, for simplicity, we use "Fz" to refer to all *frizzled*-family Wg receptors simultaneously.

Wg binding to Fz somehow causes the product of *disheveled* to suppress activity of the kinase GSK3, encoded by *shaggy*. GSK3 phosphorylates several proteins, among them the product of *armadillo* (*arm*, the *Drosophila* homolog of  $\beta$ -catenin), Daxin, and a *Drosophila* homologue of APC (reviewed by Cadigan and Nusse, '97). These three proteins form a complex which targets Arm for

ubiquitin-dependent degradation involving the product of the gene *supernumerary limbs* (Jiang and Struhl, '98). Thus Wg signaling somehow suppresses GSK3 activity, reducing Arm's affinity for Daxin and APC, allowing Arm to accumulate in the cell. Arm also binds to the *Drosophila* homologue of TCF, encoded by *pangolin* (*pan*). Arm and Pan enter the nucleus and act together as a transcriptional activator of Wg target genes, including *en* (Brunner et al., '97; van de Wetering et al., '97). In the absence of sufficient Arm, Pan may bind to the transcriptional corepressor encoded by *groucho* (Cavallo et al., '98); thus Pan may constitute a transcription switch by binding alternately to different partners, such as Ci achieves through its cleavage.

In the model "spg2" (depicted in Fig. 10), the rates at which cleavage destroys Arm varies with the occupancy of Fz by Wg, Arm binds to constitutively produced Pan, and the complex activates *en*. There is also strong evidence that Wg signaling results in the repression of *Dfz2* transcription, both in the wing imaginal disc and during segmentation, probably via Arm and Pan (Cadigan et al., '98). Variants of *spg2* included several combinations of choices (Fig. 10; Table 4), which, at the time we composed the model, could not be conclusively differentiated on the basis of empirical observations. Our interpretation of the literature tentatively leans us toward *spg2* Variant E or G as the most realistic. We report the results from a handful of other variants to show (Table 4) that none of these details makes more than a modest difference in the solution frequency, although in the model if Pan represses *en* it must not do so too avidly. It is worth noting that constraints manifest in *spg1*, on whether Wg is presented to cells or must become associated with them in order to act, are abolished with the

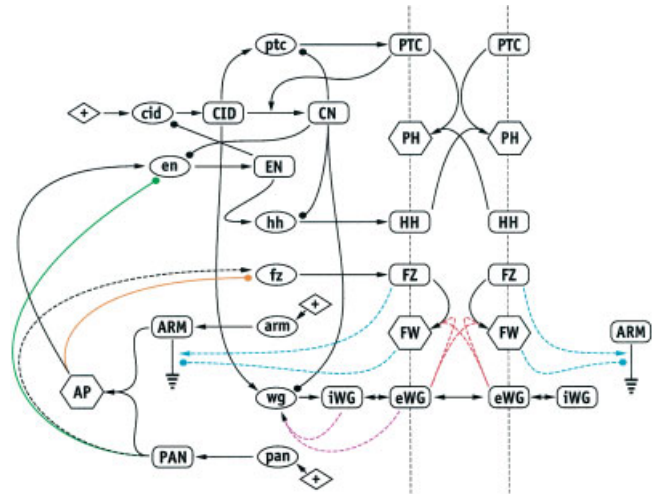


Fig. 10. Topology of *spg2*. Same diagram conventions as in Fig. 8, and again no two dashed lines of the same color exist in any one model (WG=wingless, FZ=frizzled, FW=Frizzled-Wingless complex, ARM=armadillo, PAN=pangolin, EN=engrailed, SLP=sloppy paired, HH=hedgehog, CID=cubitus ubitus interruptus (whole protein), CN=repressor fragment of cubitus interruptus, PTC=patched, PH=Patchd-Hedgehog complex). Ground symbol represents constitutive destruction of Arm at a rate regulated by Fz occupancy.

incorporation of even such a simple representation of the Wg signal transduction pathway: variants E and F are identical to B and C except for this detail. However, most startling is the fact that it is *unexpectedly easier to find solutions* for *spg2* than for the original model, *spg1*. Whereas the frequency for *spg1* and its variants tends to be around 1 in 200 or somewhat worse, the frequency for *spg2* is  $\approx 1$  in 100, despite the greater complexity of the latter model ( $75 \pm 2$  parameters, depending on the variant, versus around 50 for *spg1*, 8 loci versus five loci, and 21 species versus 13 species).

TABLE 4. Solution frequency for *spg2* variants

Variant	Distinguishing feature	No. of hits	No. of samples	Hit rate
A	Pan and Arm–Pan compete to regulate <i>fz</i> , Arm cleavage stimulated by free Fz	912	98,628	1 in 108
B	Same as A but Arm cleavage inhibited by Wg-bound Fz	1,165	129,845	1 in 111
C	Same as A but <i>fz</i> depends on Pan only	925	100,827	1 in 109
D	Same as B but <i>fz</i> depends on Pan only	1,217	124,961	1 in 103
E	Same as B but Wg binds to Fz on the same cell surface rather than opposite surfaces	1,265	130,713	1 in 103
F	Same as E but <i>fz</i> depends on Pan only	1,214	129,370	1 in 107
G	Same as E but Pan represses <i>en</i>	475	139,411	1 in 293
H	Same as F but Pan represses <i>en</i>	501	133,721	1 in 267

<sup>1</sup>Searches within a parameter space box as in Figure 6 (see also the Supplement to von Dassow et al., 2000) but with all cooperatively coefficients ranging between 1.0 and 10.0. Variants are diagrammed in Figure 10.

Clearly we require a metric by which to compare models with different numbers of parameters. A priori we expect the ease of finding solutions to go down as the parameter count rises. As complexity increases, the null hypothesis is that the more things there are to break the more likely one will fail. The null hypothesis should hold if the greater complexity comes about by intercalating features that do not inherently synergize to make each other less likely to fail, that is, if the added components are just links in a chain. Since the differences between the models spg1 and spg2 consist essentially of components added in series, we expected the null hypothesis to be validated, which would predict a lower frequency of solutions according to the chain of reasoning that follows.

The frequency is roughly the product of the probabilities that the dice throw yields a “good” value for each parameter (it is a little more subtle if parameters are correlated). For the original model with 48 free parameters and no restrictions on cooperativity (see companion paper by Meir et al., 2002, this issue), a hit rate of 1 in 250 corresponds to an average probability of about 89% per parameter of landing on a good value (48th root of  $1/250 \approx 0.89$ ). For spg2 with 75 or so parameters, a hit rate of 1 in 100 corresponds to an average probability of 94%. This does not seem an impressive difference until one works it out the other way around: if the average *per parameter* probability of a good pick were to remain constant at 89% when going from spg1 to spg2, then the hit rate for the variants of spg2 should be near 0.89 to the 73rd to 77th power, or 1 in 4,000–8,000, depending on the variant. This makes the difference between spg1 and spg2 look more dramatic. In the future we hope to devise better measures of robustness, but to date we have not been able to do so without a large investment of computation. For example, we have developed two functional measurements (Meir et al., 2002a): one in which we assess how much “mutation” the model can tolerate, and another that involves assessing the success rate of recombinants between working parameter sets. However, these methods require a great deal of computational trials and often correlate with the conclusions of the “*n*th root” formula described above, so for this paper we stick with that measure.<sup>8</sup>

<sup>8</sup>The “*n*th root” metric will deceive greatly when the parameter space encompasses many distinct basins of “working territory”. In such a case, where there are in effect many qualitatively distinct kinetic “recipes” for solving the problem, the mutational or recombinational methods will provide a much more accurate measure of the robustness of the network because they tell us how robust is a given

In contrast, the simplified version of spg1 in which mRNA and protein were collapsed together (42 free parameters) should have exhibited a solution frequency of 0.89 to the 43rd power, or 1 in 150, had it been equivalent to spg1; instead it yielded only about 1 in 1,000. If our engineered two-locus model were as robust as the core segment polarity model, we might expect 1 in 25, not  $<1$  in  $10^4$ , or 1 in 6 for the version with strict symmetry constraints instead of 1 in 150. For the architectural variants of the core model, it turns out that in most cases the decrease in solution frequency is nearly commensurate with the slight increase in parameter number, although some links (like the introduction of *slp*) appear to confer a real positive advantage on robustness; that is, those few in the latter group, as well as the increased detail represented in spg2, represent genuine improvements in the design of the network.

### Toward more complete networks

The core network model incorporates only a trivial representation of *wg* autoregulation. As we noted above, there is as yet too little information about this process for us to do much better, but *slp* seems an excellent candidate for an intermediate transcriptional regulator. *slp* has the additional and very interesting property that it engages in both a positive feedback loop with *wg* and a negative feedback loop with *en* (see discussion above in the context of spg1). Another possibility is *gooseberry*, which appears to be a target of Hh signaling through Ci (Bhat, '96; Von Ohlen et al., '97) and also a target of Wg, and which positively regulates *wg* during mid- to late embryogenesis (Li et al., '93; Li and Noll, '93). However *gsb* is known *not* to be required for early *wg* autoregulation (Hooper, '94). It is not clear at the present writing whether *slp* is stably expressed throughout embryogenesis; published reports end with mid-embryogenesis and we can't detect strong segmental expression beyond approximately stage 12 (V. Rich and G von Dassow, unpublished), but *slp* is expressed in the appropriate region in at least some segments in the adult (Struhl et al., '97). It could be that *gsb* takes over *wg* autoregulation during mid-embryogenesis. Clearly there remain significant empirical questions about how *wg* autoregulation evolves throughout

recipe. For all variants of the segment polarity network, it appears there is a single major solution basin in parameter space, albeit that basin is fed by many rivulets and side canyons and wash-gullies. Thus for this network the “*n*th root” seems adequate.

embryogenesis, questions which need to be resolved before we can confidently incorporate any credible solution in a model.

In the core network we modeled Ptc as a direct modulator of Ci cleavage, which it is not. In reality Ptc is a stoichiometric inhibitor of the transmembrane protein encoded by *smoothened* (Alcedo et al., '96; Alcedo and Noll, '97; Chen and Struhl, '98). In the absence of Ptc, Smo transduces a constitutive signal that stabilizes Ci by regulating its association in a complex with several other proteins including the Fu protein kinase, the product of *Suppressor of fused*, and the kinesin-like protein encoded by *costal-2* (Robbins et al., '97; Sisson et al., '97). This complex both prevents full-length Ci (but not CN) from entering the nucleus and also directs Ci to proteolysis which converts it to CN. Ptc binding to Smo prevents Smo from signaling; Hh binding to Ptc prevents Ptc from binding Smo; thus, Hh titrates away Ptc, allowing Smo to send its signal, resulting in the accumulation of full-length Ci. Protein Kinase A also regulates Ci: phosphorylation by PKA may modulate Ci binding to Fu, Su(fu), and Cos2, may modulate Ci cleavability, and may influence the ability of Ci to enter the nucleus and activate its targets (Chen et al., '98; Wang and Holmgren, '99). Unfortunately, it is not apparent yet whether or how Hh (or anything else during segmentation) might influence PKA; the current suggestion places Smo and PKA on parallel pathways.

As steps toward a more realistic framework for further exploring the segment polarity architecture we tested the models "spg3" and "spg4," extensions of spg2 which we do not discuss in detail here. Spg3 attempted to account for *wg* auto-regulation via Fused and Ci instead of through *slp*, and was unsuccessful. Spg4 incorporates *smo* and drops the assumption of irreversible hetero-dimerizations; all complexes are allowed to dissociate. Spg4d, the variant most comparable to the original model, is governed by 84 free parameters. In 40,326 random samples we found 386 solutions (1 in 104). The null hypothesis would have predicted roughly 1 in 20,000 if the greater complexity of spg4 compared to spg1 did nothing specific to improve the outcome.

## Summary

Figure 11 shows graphically how the various models compare; to summarize, whereas a null hypothesis would predict that increasing the level

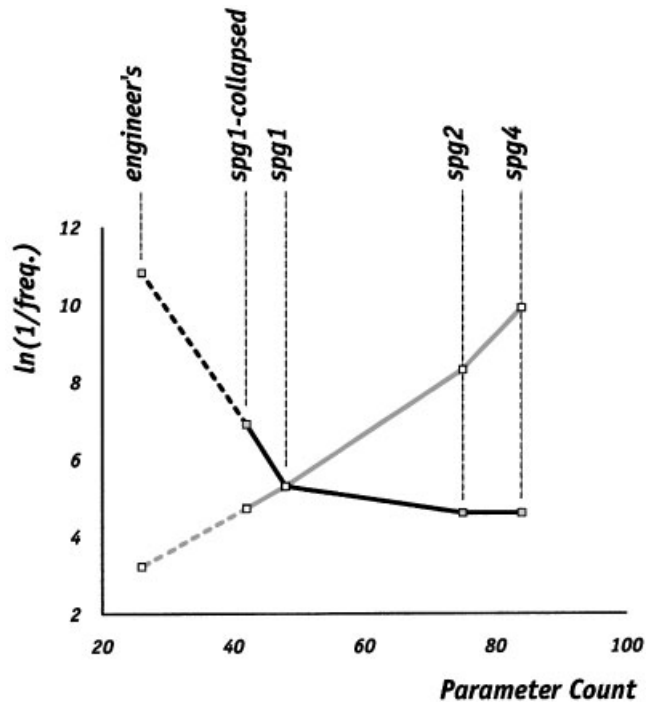


Fig. 11. Fragility of segment polarity network models as a function of complexity. Plotted here is the natural log of 1 over the solution frequency for several models, versus the number of free parameters in each model. The quantity on the vertical axis gives a rough answer to the question, "how hard is it to find parameter sets that make the model work?" The stippled line represents the null hypothesis, discussed in the main text. The solid line plots the actual results for segment polarity models that incorporate a progressively greater level of intermediate detail, as reflected in the parameter count. Also included is the engineered network (described in Fig. 9) which is the most fragile of all, despite its simplicity.

of detail in the model would make it harder to find working parameter sets in a random search, in fact, for this network, adding known details makes it easier to find solutions in parameter space, with respect to the boundary-maintenance task that we consider to be the fundamental biological role of the segment polarity network. However, spg4 (and more complex versions not discussed here) begins to show signs of a certain complexity burden. In a way, in spg4 the various cell states that make up the desired pattern are *too* stable. It seems that spg4 embodies, in effect, many different kinetic mechanisms for stabilizing the target pattern, all of which overlap in parameter space. On the one hand, this makes this network even more robust than simpler approximations, but on the other hand, it also means

A

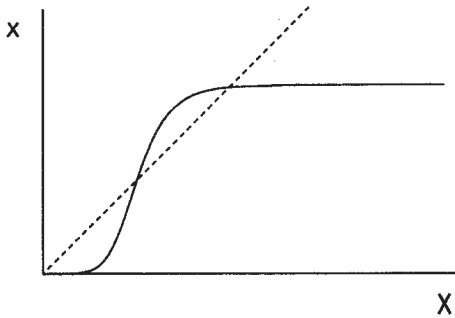
$$\frac{dx}{dt} = T_{\max} \rho_x \left( \frac{X^{v_{Xx}}}{\kappa_{Xx}^{v_{Xx}} + X^{v_{Xx}}} \right) - \frac{x}{H_x}$$

$$\frac{dX}{dt} = P_{\max} \sigma_x X - \frac{X}{H_x}$$

E

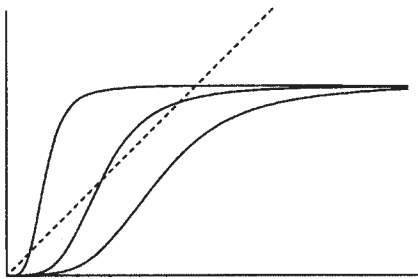
$$\frac{dx}{dt} = T_{\max} \rho_x \left( \frac{\alpha \left( \frac{X^{v_{Xx}}}{\kappa_{Xx}^{v_{Xx}} + X^{v_{Xx}}} \right) + \beta \left( \frac{Y^{v_{Yx}}}{\kappa_{Yx}^{v_{Yx}} + Y^{v_{Yx}}} \right)}{1 + \alpha \left( \frac{X^{v_{Xx}}}{\kappa_{Xx}^{v_{Xx}} + X^{v_{Xx}}} \right) + \beta \left( \frac{Y^{v_{Yx}}}{\kappa_{Yx}^{v_{Yx}} + Y^{v_{Yx}}} \right)} \right) - \frac{x}{H_x}$$

B



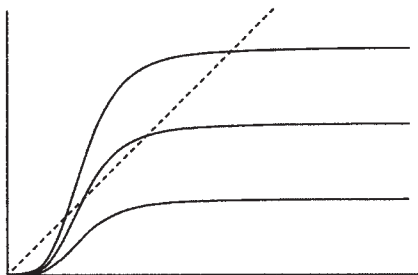
C

$T\rho=1.0, \kappa_{Xx}=\{0.2,0.5,0.8\}, v_{Xx}=4.0$



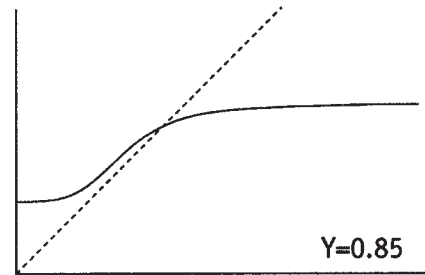
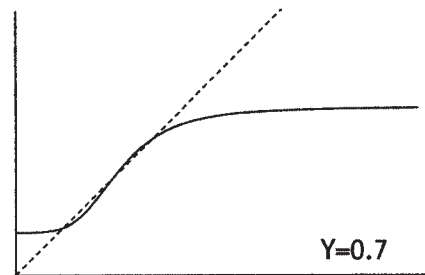
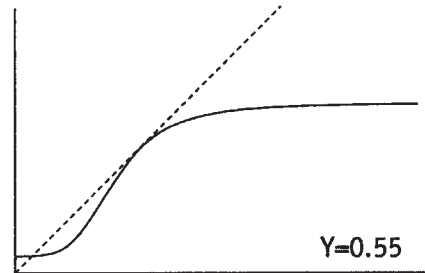
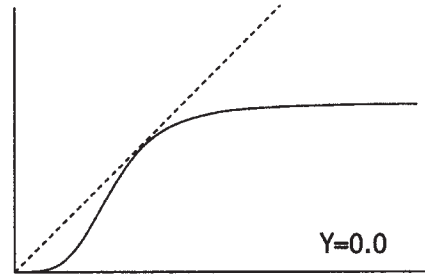
D

$T\rho=\{0.6,0.8,1.2\}, \kappa_{Xx}=0.4, v_{Xx}=4.0$



F

$T\rho=1.0$   
 $\alpha=8.0$   
 $\kappa_{Xx}=0.9$   
 $v_{Xx}=4.0$   
 $\beta=2.0$   
 $\kappa_{Yx}=1.0$   
 $v_{Yx}=5.0$



it is a much less dynamic network. Cell states in *spg4* appear to be so much more self-reinforcing than in *spg1* that it is very difficult to perturb the model once it locks in on a particular spatial pattern of cell states.

#### Section IV: Stripe sharpening, a dynamic function

Segment polarity genes are expressed in dynamic patterns. For example, stripes of expression of both *wg* and *en* are widely reported to narrow as the germ band extends in the 3.5- to 5.0-hr old *Drosophila* embryo. Also, in the early *Drosophila* embryo cephalic segments differ from the trunk segments in the detailed patterns of segment polarity gene expression and in their mutual dependencies (Gallitano-Mendel and Finkelstein, '97); even between dorsal, lateral, and ventral regions of the trunk segments there may be major differences, since *wg* expression only persists beyond germ-band extension in the ventral neurogenic ectoderm. In this section we challenge the model to mimic the reported narrowing of *wg*- and *en*-expressing stripes during germ-band extension.

#### Sharpening the wingless stripe

All models described above failed to account for how the stripe of *wg* expression sharpens during germ band extension. As the germ band extends, cell rearrangement causes each segment to expand

along the anterior–posterior axis from 4 cells wide to roughly 8 cells wide; by stage 12 each segment, after the combined effects of cell division, rearrangement, and neuroblast ingression, is about 12 cells wide in the epidermal layer. Throughout, the *wg* stripe remains only one cell wide. Thus, cells that once expressed *wg* must turn it off as they move too far from the influence of Hh-producing cells. None of our models could account for how *wg*, once activated, could turn off, since *wg* autoregulation plays such an important role in the most fundamental behavior of the network. In all the models described so far, Wg autoregulatory and Ci/CN pathways effect *wg* expression additively. That is, to be conservative we assumed that these pathways were completely different and had no positive or negative influence on each other. Hooper ('94) interpreted some of her results to mean that these pathway synergize, but did not specifically distinguish between additive and synergistic models, so in the absence of a molecular mechanism for *wg* autoregulation we stuck with an additive model as the simplest possibility.

Analysis of nullclines in Figure 12 shows the problem. Figure 12A and B show generic equations for a self-activating gene product and the nullclines for those equations, respectively. For *wg* autoregulation to provide the asymmetry for which it was introduced to the model (von Dassow et al., 2000), the differential equations governing *wg* products must, in the absence of any other factors, have two stable steady states: *wg* off and *wg* on, corresponding to the lower- and uppermost




Fig. 12. Simple equations and nullclines for an autoregulatory gene. (A) Boilerplate equations in which the product of gene *x* activates further *x* mRNA synthesis according to a sigmoid dose–response curve. X protein is translated according to a simple unregulated formula. Both species exhibit first-order decay. (B) Nullclines for the system of equations in panel A. Nullclines are made by setting the derivatives to zero and plotting the formula when solved for *x* mRNA (black line) as a function of X protein, or X protein as a function of *x* mRNA (dashed line). Where the nullclines cross, both derivatives are zero and the system is at steady state. Analysis of eigenvalues of the Jacobian matrix determines whether the steady state is stable, and it is a trivial matter to show that, in panel B, the “off” state is stable and the “on” state is stable. The state in between is unstable and lies along the line (called a “separatrix”) dividing the basins of attraction for the two stable steady states. Above the separatrix, the system will evolve *inevitably unless perturbed across the separatrix* to the “on” state, below it to the “off” state. The position of the second crossing-point along the X nullcline is an easy gauge for the “switching threshold.” Such a system is *bistable*. (C)

Effect of varying the half-maximal coefficient. Such an effect, an increase in  $\kappa_{xx}$ , might be accomplished by some synergistic transcriptional coactivator that participates by binding to X and altering its conformation to improve its affinity for binding sites in the *x* enhancer. (D) Effect on the system in panel A of varying the top line. Such an effect might be achieved by a cofactor that regulates the ability of X to recruit transcriptional machinery to the promoter. In C and D the “off” state is always preserved. In contrast, an additively autoregulating gene is probably very hard to turn off once it gets turned on. (E) Simple additive model of an autoregulatory enhancer region in which both X and Y contribute, independently, to transcriptional activation of *x*. See Appendix A to the companion paper by Meir et al. (2002b, this issue) for a comparison with other formulas. (F) Nullclines for a system involving the equation for the derivative of *x* mRNA in panel E, and the equation for X protein in panel A, showing the effect of varying the concentration of Y given the parameters shown. Only in a narrow window, and only for carefully chosen parameter values, is the whole system ever bistable, and even then the “off” state is not completely off.

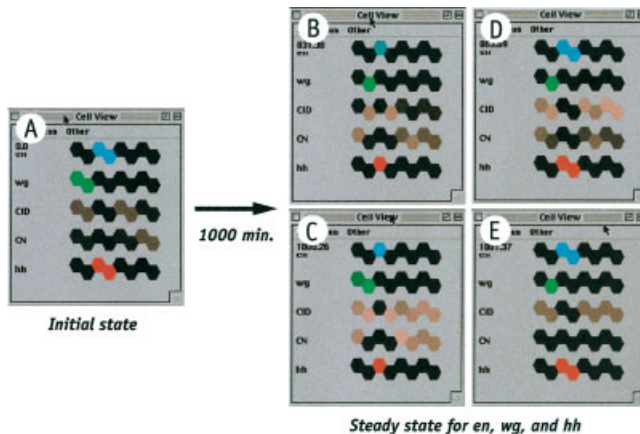


Fig. 13. Synergistic model allows *wg* stripes to narrow. (A) Initial state for stripe-sharpening test. This pattern is a stereotype of what each segment might look like immediately after germ band extension: cell rearrangements make the segment almost twice as wide along the anterior-posterior axis, causing *en*-expressing cells and *wg*-expressing cells to move away from the parasegmental boundary either posteriorly or anteriorly, respectively. Starting with this initial pattern we test whether parameter sets that succeed at the standard boundary-maintenance task enable the model to turn off *wg* or *en* expression in cells that “no longer” abut the parasegment boundary directly. Not shown, but also included in the test pattern, are *Wg*, *En*, and *Hh* levels corresponding to the mRNA concentrations shown here, and also modest levels of *ptc* mRNA and protein in cells 1, 2, 5, and 6, numbered from the left. (B–E) Four out of 21 parameter sets we found (see text) that enable *wg* stripe sharpening. Some parameter sets allow both the *wg* and *en* stripes to sharpen (as in B and C). Some parameter sets (as in C) only enable the model to reduce, but not completely eliminate, *wg* expression in cells not immediately adjacent to *Hh*-producing cells. Most of the successful sets accomplish *wg* sharpening by achieving a quasi-stable difference in the relative abundance of full-length *Ci* (*CID*) and the N-terminal repressor (*CN*), as in B–D. A few, however, do not: in E, the steady-state pattern of *Ci* and *CN* is uniform in all non-*en*-expressing cells, but the *wg* stripe sharpens because, during the initial transients, *Ci* accumulates too slowly in the distal cells to “save” *wg* expression.

crossings in Figure 12B. The middle crossing is an unstable steady state that lies on the line separating basins of attraction for the two stable steady states. This picture is the basis for the absolute requirement that the response of *wg* to *Wg* signaling must be cooperative (see companion paper by Meir et al., 2002b, this issue). If *Ci* acts additively, it can only shift upward the baseline on the solid curve in Figure 12F, eventually destabilizing the “off” state completely. Considering the formula in Figure 12A, there are several other possible ways that *Ci*/*CN* could interact with *Wg* (see Fig. A4 in Appendix A to the companion paper by Meir et al., 2002b, this issue): *Ci* could

synergize with *Wg* either by shifting up the top line (Fig. 12C), or by shifting left the inflection point (Fig. 12D).

In order for the boundary to be asymmetric, whatever happens in the presence of high *Wg* on the anterior side of the compartment boundary must not happen on the posterior of the *en*-expressing row (where *Ci* is also elevated) in the initial absence of high *Wg*. That is fine as long as *Wg* can sustain itself by autoregulation. However, this condition prevents stripe sharpening for an additive model, and furthermore it may be wrong: in fly embryos *Ci* is absolutely required for *wg* expression although by itself it is only able to weakly activate *wg* (Hooper, '94). In the models presented so far, this is not so; *Ci* is usually only required in the models (and not even in every case) to keep *wg* on during an initial period. Indeed, given the additive model it is difficult to find parameters such that *Ci* would be required for *wg* expression and yet not be able to activate *wg* posteriorly (especially if *Wg* diffuses at all), hence the preference that *Ci* be a poor activator and *CN* a good inhibitor of *wg* (Fig. 6).

The reason this poisons stripe sharpening is that, if *Wg* is a good activator of itself, as cells move away from the *Hh*-producing region they will experience no deficit if *CN* only acts as a competitive antagonist of full-length *Ci*. Thus, with a purely additive model of the *wg* enhancer region, once *wg* turns on it stays on no matter what in all but a narrow crevice of parameter space. That crevice, part of which is illustrated in Figure 12F, requires exquisitely fine tuning. *CN* cannot turn off *wg* unless *Wg* is just barely too weak to keep itself on in the absence of an assist from *Ci*. Even if it is possible, we could never have found it in a random search: the right conditions are exquisitely sensitive to half a dozen or more parameters.

These problems evaporate if *Ci* and *Wg* synergistically activate *wg*. Many synergistic mechanisms are plausible: *Wg* could promote its own expression, for example, by stimulating *Ci* to become a better activator of *wg*; alternatively, *Wg* signaling could result in the expression or activation of some other factor such as *Slp*; *Slp* could synergize with *Ci* at the level of enhancer binding, or transcriptional activation of *wg* could require some collaboration between several proteins recruited by various independently binding transcription factors. We tested a version of *spg1* using a simple synergistic formula for the regulation of *wg* transcription. In a search



of 163,875 random parameter sets, we found 276 parameter sets for which the model meets the standard test of holding the boundary; for 21 of those parameter sets, the model was able to effect the narrowing of a two-cell-wide *wg* stripe to only one cell wide. That is, under these 21 parameter sets, when challenged with an initial prepatter intended to stereotype the state of gene expression just at the end of the fast phase of germ-band extension (see Fig. 13), the model completely shut down *wg* in the row of cells 1 cell diameter away from the Hh-producing cells, leaving only a one-cell-wide *wg* stripe. This is not a remarkable showing; it corresponds to only  $\approx 1$  in  $10^4$ . However, this was a very crude test, and we expect that as details of the *wg* autoregulation mechanism emerge, we will be able to improve the model's performance on this test.

For many of the results described in the first three sections of this chapter we have tested whether our conclusions depend on the choice of an additive or a synergistic model, and they do not. It is a matter for empirical investigation whether Wg and Ci synergize, and how. There are various reasons to favor an additive model. In particular, Ci drives transcription from the *wg* enhancer in cultured cells, presumably in the absence of whatever factors are involved in *wg* autoregulation (Von Ohlen et al., '97). In embryos in which Wg signaling is prevented, low levels of *wg* are expressed, presumably under the control of Ci (Hooper, '94). From Figure 12C and D it is evident that a simple synergistic model could not account for this. On the other hand, in embryos the fact that *wg* expression is absolutely dependent on Ci suggests a synergistic mechanism of some sort. Our model shows that there are major functional consequences for this choice, at least with respect to stripe sharpening, and that if Ci and Wg do not synergize then something big is likely to be missing from the model. A possibility, if Ci and Wg do not synergize but instead act additively, is that Wg signaling may become highly localized to the compartment boundary vicinity through local expression or biased intracellular localization of co-receptors and other proteins required for Wg signal transduction.

### Sharpening the engrailed stripe

Based on an elegant cell-marking study, Vincent and O'Farrell ('92) showed that cells lose *en* expression as they move away from the paraseg-

ment boundary during germ-band extension. Vincent and Lawrence ('94) showed that this is because the Wg signal travels only over a very short range, as little as 1 cell diameter. The core network (spg1) had little difficulty with the task of sharpening the *en* stripe in the same tests described above. As many as one-third of the solutions for spg1-grade models were capable of sharpening the *en* stripe from two cells to one cell wide. To our dismay, we found that more complex models (spg2 and spg4 and others) have a much harder time with this test. We watched spg4d run with hundreds of different solutions, *only one* of which enabled this model to sharpen a 2-cell-wide *en* stripe to one cell wide. It was very rare for the model to achieve uneven distributions of Pan versus the Arm–Pan complex. In fact, despite localized Wg production, only a minority of solutions enabled the model to achieve spatially varying distributions of the Fz–Wg complex; without spatially varying Fz occupancy, no spatial variation in Arm cleavage will arise, and no spatial regime of Pan versus Arm–Pan complex levels is possible. How, then, is *en* expression confined to a stripe at all in spg4, never mind how it sharpens?

Consider the interactions of Wg and Fz and Arm and Pan: they bind to each other stoichiometrically. We allow the maximum level of proteins in our models to range from  $10^3$  to  $10^6$  copies per cell (see Supplementary Information to von Dassow et al., 2000, for the rationale). Considering two proteins that bind to each other, in the standard parameter space box we use, only a small sliver will exist where those proteins have the same maximum expression level. If the two proteins have widely different concentrations in the cell, the excess of one may completely swamp the other. This is the basis for ligand buffering between any kind of interacting entities, from protons to people. Imagine that Arm, for instance, can accumulate to a tenfold higher level than Pan, and that Arm and Pan bind with reasonably high affinity. Then, even if the concentration of Arm is half maximal in one cell but maximal in the others, the concentration of the complex will be nearly the same in both cells.

But then, how is it that *en* is not expressed ubiquitously as well under such conditions? In the model, transcription of *en* is regulated by both the Arm–Pan complex and by CN; meanwhile, En prevents expression of *ci*. The CN–En double negative requires a positive input if it is to be a bistable switch: both *arm* and *pan* are expressed ubiquitously, and if they are not stoichiometrically

matched then it is possible that they merely provide a basal input to *en*. In that case, once *en* gets turned on, it keeps itself on by repressing its only repressor, *ci*. Wg signaling would be required only initially, as *en* expression ramps up. Indeed this may explain two phenomena about the segment polarity network. There is only a relatively short window of time during which *en* is dependent on Wg signaling, and that is during germ band extension as the expression of both genes is still below maximum. Second, Heemskerk showed that heat-shock induced ectopic expression of *en* after germ-band extension could cause an expansion of the *en* stripe (Heemskerk et al., '91). Historically this result was taken to indicate that En activates its own production. However, it could be instead that the heat-shock induced En merely shuts down *ci* expression, and that by late germ-band extension there is sufficient Arm and Pan that excess En “throws the switch” and is henceforth clonally inherited (see Fig. 14D).

These considerations suggest how to achieve stripe sharpening. Arm and Pan should be basally expressed at similar levels and be able to accumulate to nearly the same maximal cellular concentration, and perhaps Wg and Fz should be likewise constrained. Furthermore, we wondered whether, in this context, it would help sharpen the stripe if free Pan were to act as a repressor of *en*. It turns out that only stoichiometric balancing of Arm and Pan matters. Since automated screening methods have not yet given us reliable results with the stripe-sharpening challenge, we resorted to screening the model's behavior by eye. We began by collecting automatically, for several variants of *spg4d*, several hundred solutions that pass the standard 4-cell-wide pattern-holding test. We then challenged them with the 8-cell-wide “germ band extended” test (Fig. 13) and watched how the model behaved over a 1,000-min period when governed by each of those parameter sets. For *spg4d* itself, we screened a first catch of >600 solutions and found only one that sharpened the *en* stripe (i.e., the posterior *en* cell turned off both *en* and *hh* completely, replacing them with a cell state in which full-length Ci and *ptc* were both abundantly expressed). In one other case, the posterior *en* cell merely came to express *en* at a reduced level compared to the cell immediately adjacent to the Wg-producing cells. This shows that *spg4d* is capable, intrinsically, of accomplishing this task, but the frequency is on the order of 1 in  $10^5$  or less.

We conducted identical screenings with variants of *spg4d* that introduced either constraints on the

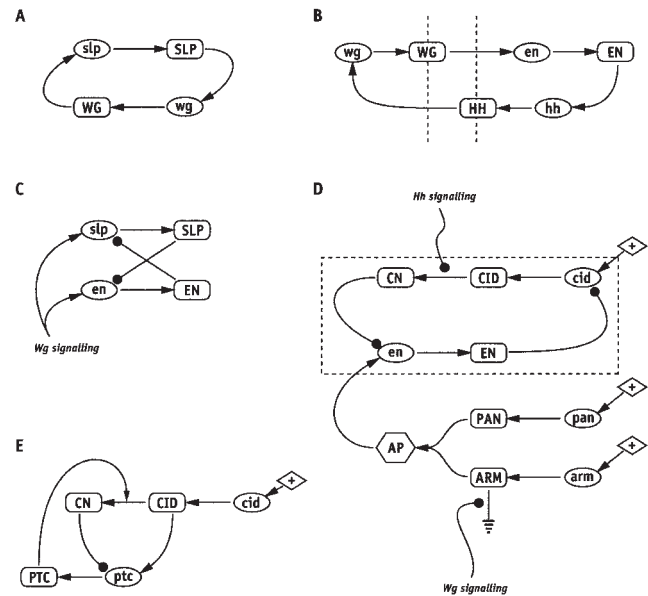


Fig. 14. Elements of the segment polarity network. Individual panels here represent subsets of the connections in Figs. 8 and 10, some of them abbreviated. (A) Positive feedback between *slp* and *wg* makes a bistable switch which, like the simplistic example in Fig. 2, could have two stable steady states, both components on or both off, with a threshold for turning on or off. (B) Similar to A, mutual activation between *wg*, *en*, and *hh* potentially creates another bistable switch. (C) Mutual repression between *slp* and *en*, when combined with a positive input to each, makes an exclusive-or switch in which one or the other can be expressed at a level determined by the input (in this case provided by Wg signaling). (D) The mutual repression we hypothesize between *ci* and *en* would also make an exclusive-or switch (enclosed in the dashed box), but in this case the positive inputs to each side of the switch are independently adjustable, unless otherwise coupled (as they are in the context of the whole circuit). This sub-circuit might explain how the *en* expressing cell state becomes self-sustaining at the end of germ-band extension (CIT Heemskerk); if sufficient Arm–Pan complex accumulates in the absence of Wg signaling, then pre-existing high-level En in the cell might prevent repressors, such as *slp* and possible *ci*, from accumulating in the same cell. This hypothesis could be tested by replicating Heemskerk's *hs-en* experiments in a genetic background in which the expected background level of the Arm–Pan complex was reduced. (E) Interactions between the products of *ptc* and *ci* constitute a homeostat—these components participate in a feedback loop with a single negative interaction: the more Ptc is produced in response to full-length Ci protein, the more Ci is converted to CN, not only depleting Ci but also repressing *ptc* transcription. If *ci* is basally expressed, as it is in the models discussed here, then negative feedback leads to a stable steady state with some intermediate level of *ptc* expression, neither fully expressed nor fully repressed. Hh protein binds to and titrates away Ptc; thus Hh tunes the homeostat, just as we adjust the household thermostat. Titrating away Ptc decreases Ci cleavage rate, consequently increasing the steady-state *ptc* expression level. In addition increased Ptc expression soaks up Hh, as long as Ptc can accumulate to a level commensurate with the pool of Hh available for binding.

relative expression levels of Arm and Pan, or additional similar constraints on Wg and Fz, or the postulated repressive link between Pan and *en*. When imposing the first of these constraints, out of  $3 \times 10^4$  random samples, we found 6 that exhibited some evidence of *en* stripe sharpening, 3 of which completely turned off *en* in the cell further from the Wg source. This is about an order of magnitude more frequent (at least) than for *spg4d* (6 in  $3 \times 10^4$  vs. 2 in  $6 \times 10^5$ ). Other constraints on stoichiometry reduced rather than improved the frequency, and the Pan-*en* link had no detectable effect. Thus, we could patch up our model to make it behave as we desired, but the constraint introduced is a serious one, and even with it the model does not perform exceptionally well at this test.

### Summary

For the model to exhibit sharpening of the *wg* and *en* stripes we had to impose, in the first instance, a specific mechanism for combining two regulatory pathways that feed into *wg* transcription, and in the second instance, a constraint that the two components of the crucial transcriptional switch that mediates *en* activation must be expressed at nearly equal levels. We are currently investigating *en* stripe sharpening in real embryos. We find that En expression increases at least 5-fold during germ-band extension and, furthermore, that En is expressed in one-cell-wide stripes only transiently, if ever (V. Rich and G. von Dassow, unpublished). Nevertheless, comparing an En-GFP reporter with En antibody staining shows that some cells do appear to lose *en* expression on the posterior edge of the stripe, confirming Vincent and O'Farrell's ('92) results (V. Rich and G. von Dassow, unpublished). Thus it may be that cells that are on their way to, but have *not yet* achieved, full *en* expression fail to maintain it as they move posteriorly. Whatever the answer, from the modeling perspective what is important is that we had difficulty getting a simple model of the Wg pathway *simply to turn off*. Of course future, more faithful models might erase this difficulty. Regardless, the same difficulty with stoichiometric balancing is likely to afflict many similar signaling processes that rely on regulating relative availability of binding partners.

### CONCLUSIONS

In this paper we sought to take known facts or hypotheses, incorporate them into our working

model of the segment polarity gene network, and assess how the model's behavior alters in response. That is, we have engaged here in what Lawrence and Sampedro ('93), quoting Crick, call "carpentry." Lawrence and Sampedro criticized early attempts to synthesize facts about *Drosophila* segmentation in terms of causal chains of interactions among individual genes. They remark that the carpentry approach to synthesis often results in circular or self-contradictory and ad hoc collections of predicates, and they proposed instead to conceive of the segment-patterning process in terms of gradients, abstracted from the specific activities of particular molecules in determining cell states within the segment. Lawrence and Sampedro articulated an aesthetically and phenomenologically satisfying hypothesis without substantial recourse to what even then was remarkable knowledge of the molecular nature of segment polarity genes and their interactions. However, their account, by its very nature, provides no synthesis of the disparate facts of molecular genetic analysis and thus seems unsatisfying to someone attempting to fit together the molecular puzzle pieces.

The problem with the carpentry that Lawrence and Sampedro derided is that it consisted of verbal reasoning only. This paper represents an attempt to formalize carpentry, using computers to solve differential equations that characterize the genetic interactions inferred by molecular geneticists. Whatever else one can say about the usefulness of models of complex systems, computers *are not* fooled by circularity and logical contradictions, and thus the computer model lets us conduct a kind of reconstitution experiment with the known facts about the process of interest. This exercise yields three pragmatic results: first, a set of empirically testable predictions about the specific real network expressed in the models; second, general predictions about the emergence of systems-level properties of gene regulatory networks; and third, a platform from which to explore the evolvability of developmental mechanisms, hopefully developing a bridge across the conceptual gap between mechanistic analysis of development and population-level studies of variation and variability.

In addition, the reconstitution exercise reveals how simple elements, such as positive and negative feedback loops, with readily understood dynamical properties conspire to form a larger mechanism. The segment polarity *model* consists of several intertwined dynamical elements, as

shown in Figure 14. It includes at least two positive feedback loops that, separately, could exhibit bistable on/off switch-like function: *wg* auto-activation, likely via *slp* (Fig. 14A), and the mutual promotion of *wg* and *en* expression (Fig. 14B). In addition there are at least two pairwise cross-inhibitions which, given some positive input to each component, ought to behave as either/or switches: mutual inhibition between *en* and *slp* (Fig. 14C), and the hypothetical mutual inhibition by *ci* and *en* (Fig. 14D). In the former case, Wg signaling provides a common positive input to each gene, and in the latter case either basal expression or, again, Wg signaling provides the necessary input. Finally, the model incorporates a single negative feedback loop between *ci* and *ptc* that could act as a homeostat (Fig. 14E).

The first two dynamical elements in Figure 14 promote stabilization of *wg*-expressing and *en*-expressing cell states, respectively, assuming permissive conditions for each state. For example, in the case of Figure 14A, the permissive conditions would be that there be too little CN present to repress *wg*, and that there be too little En present to repress *slp*. The next two elements ensure mutual exclusivity of *wg*- and *en*-expressing cell states; note that a cell state expressing both *wg* and *en* becomes possible if parameters are tuned such that En is a weak repressor of *slp*, Slp is a strong activator of *wg* but a weak repressor of *en*, and either Ci is not required for *wg* expression or En only weakly represses *ci*. The *ci-ptc* homeostat maintains the responsiveness of a ground state and also, depending on the relative level of expression of Hh and Ptc, buffers Hh concentration within the vicinity of its source. Furthermore, if Arm and Pan concentrations are tuned such that there is little or no basal activation of *en*, and if Ci is actually required for *wg* activation, then the ground state can “invade” either the *wg*- or the *en*-expressing cell state, should the factors sustaining those states fade (i.e., as the germ band extends). At least, that’s how the *model* works.

This conception of the segment polarity module as a system of mutually entrained cell state switches explains how a global “design” feature, the level of cooperativity in regulatory interactions, confers upon the network robustness to variation in parameters, to initial conditions, or to noise. Increasing cooperativity promotes switch-like behavior in the dynamical elements diagrammed in Figure 14A–D. Looking at it the other way around, with *low* cooperativities throughout

these switching elements, the cell states that define the model’s functional behavior become, in a sense, more elastic. Thus, for example, at low cooperativity the entire network “rings” in response to oscillations generated in the *ci-ptc* loop, or in response to noise, thus disrupting the maintenance of a stable spatial regime of cell states. In the same way, at low cooperativity the network’s steady states “stretch” easily in response to changes in parameters.

Genetic mutations and environmental variation both correspond to coordinated changes in some subset of parameter values. Any mutation of a particular locus in the network corresponds to a move along some diagonal in parameter space. Similarly, an environmental perturbation such as a change in temperature corresponds to a move along some (other) diagonal in parameter space. Developmental noise might correspond to a random walk, over the course of development, along arbitrary diagonals. (One must also think of any change in initial conditions as an equivalent perturbation.) Increasing cooperativity within the dynamical elements shown in Figure 14A–D increases the tolerance of the network to moves along *any* diagonal in parameter space. This suggests that switching networks such as this one epitomize a congruence, in the sense of Ance and Fontana (2000), between robustness to the three major categories of insult that physiological mechanisms confront.

Population genetic models show that while it may be relatively straightforward to select for canalization against environmental perturbations, it is difficult to concoct an analogous scenario for genetic canalization (Wagner et al., ’97; Gibson and Wagner, 2000). The apparent plastogenetic congruence manifest in the segment polarity model, and also in our model of the neurogenic network (Meir et al., 2002a), raises the possibility that genetic canalization might emerge as a byproduct of selection for robustness to environmental perturbation. More generally, these considerations make us hopeful that models like these can provide an interpretive metaphor to explore the mechanistic origins of systems-level properties of genetic architecture, such as epistasis, canalization, and dominance, which until recently have been necessarily treated as black boxes in evolutionary theory.

## ACKNOWLEDGMENTS

Thanks to Richard Strathmann for comments on an early draft of the manuscript, to Virginia

Rich for comments and proofreading, and to Eli Meir and Dara Lehman for suggestions and advice that contributed to the work described here. This work was supported by the National Science Foundation (MCB-9732702, MCB-9817081, and MCB-0090835) to GMO. The main body of this paper, in modified form, was previously published as part of GvD's doctoral thesis (University of Washington Department of Zoology, 2000). The work described here was primarily conducted while in residence at Friday Harbor Laboratories, and we thank the director, Dennis Willows, for accommodating us.

### LITERATURE CITED

- Akimaru H, Chen Y, Dai P, Hou DX, Nonaka M, Smolik SM, Armstrong S, Goodman RH, Ishii S. 1997. *Drosophila* CBP is a co-activator of cubitus interruptus in hedgehog signalling. *Nature* 386:735–738.
- Alcedo J, Noll M. 1997. Hedgehog and its patched-smoothened receptor complex: a novel signalling mechanism at the cell surface. *Biol Chem* 378:583–590.
- Alcedo J, Ayzenzon M, Von Ohlen T, Noll M, Hooper JE. 1996. The *Drosophila* smoothened gene encodes a seven-pass membrane protein, a putative receptor for the hedgehog signal. *Cell* 86:221–232.
- Alexandre C, Jacinto A, Ingham PW. 1996. Transcriptional activation of hedgehog target genes in *Drosophila* is mediated directly by the cubitus interruptus protein, a member of the GLI family of zinc finger DNA-binding proteins. *Genes Dev* 10:2003–2013.
- Alves G, Limbourg-Bouchon B, Tricoire H, Brissard-Zahraoui J, Lamour-Isnard C, Busson D. 1998. Modulation of Hedgehog target gene expression by the Fused serine-threonine kinase in wing imaginal discs. *Mech Dev* 78:17–31.
- Ancel LW, Fontana W. 2000. Plasticity, evolvability, and modularity in RNA. *J Exp Zool (Mol Dev Evol)* 288:242–283.
- Anderson DT. 1973. Embryology and phylogeny in annelids and arthropods. New York: Pergamon Press. xiv, 495 pp.
- Aza-Blanc P, Ramirez-Weber FA, Laget MP, Schwartz C, Kornberg TB. 1997. Proteolysis that is inhibited by hedgehog targets Cubitus interruptus protein to the nucleus and converts it to a repressor. *Cell* 89:1043–1053.
- Bellaiche Y, The I, Perrimon N. 1998. Tout-velu is a *Drosophila* homologue of the putative tumour suppressor EXT-1 and is needed for Hh diffusion. *Nature* 394:85–88.
- Bhanot P, Brink M, Samos CH, Hsieh JC, Wang Y, Macke JP, Andrew D, Nathans J, Nusse R. 1996. A new member of the frizzled family from *Drosophila* functions as a Wingless receptor. *Nature* 382:225–230.
- Bhanot P, Fish M, Jemison JA, Nusse R, Nathans J, Cadigan KM. 1999. Frizzled and DFrizzled-2 function as redundant receptors for Wingless during *Drosophila* embryonic development. *Development* 126:4175–4186.
- Bhat KM. 1996. The patched signaling pathway mediates repression of gooseberry allowing neuroblast specification by wingless during *Drosophila* neurogenesis. *Development* 122:2921–2932.
- Bhat KM. 1998. frizzled and frizzled 2 play a partially redundant role in wingless signaling and have similar requirements to wingless in neurogenesis. *Cell* 95:1027–1036.
- Bhat KM, van Beers EH, Bhat P. 2000. Sloppy paired acts as the downstream target of wingless in the *Drosophila* CNS and interaction between sloppy paired and gooseberry inhibits sloppy paired during neurogenesis. *Development* 127:655–665.
- Blair SS, Ralston A. 1997. Smoothened-mediated Hedgehog signalling is required for the maintenance of the anterior-posterior lineage restriction in the developing wing of *Drosophila*. *Development* 124:4053–4063.
- Brown SJ, Hilgenfeld RB, Denell RE. 1994. The beetle *Tribolium castaneum* has a fushi tarazu homolog expressed in stripes during segmentation. *Proc Natl Acad Sci U S A* 91:12922–12926.
- Brown SJ, Parrish JK, Beeman RW, Denell RE. 1997. Molecular characterization and embryonic expression of the even-skipped ortholog of *Tribolium castaneum*. *Mech Dev* 61:165–173.
- Brunner E, Peter O, Schweizer L, Basler K. 1997. pangolin encodes a Lef-1 homologue that acts downstream of Armadillo to transduce the Wingless signal in *Drosophila*. *Nature* 385:829–833.
- Burke R, Nellen D, Bellotto M, Hafen E, Senti KA, Dickson BJ, Basler K. 1999. Dispatched, a novel sterol-sensing domain protein dedicated to the release of cholesterol-modified hedgehog from signaling cells. *Cell* 99:803–815.
- Cadigan KM, Nusse R. 1997. Wnt signaling: a common theme in animal development. *Genes Dev* 11:3286–3305.
- Cadigan KM, Grossniklaus U, Gehring WJ. 1994a. Functional redundancy: the respective roles of the two sloppy paired genes in *Drosophila* segmentation. *Proc Natl Acad Sci U S A* 91:6324–6328.
- Cadigan KM, Grossniklaus U, Gehring WJ. 1994b. Localized expression of sloppy paired protein maintains the polarity of *Drosophila* parasegments. *Genes Dev* 8:899–913.
- Cadigan KM, Fish MP, Rulifson EJ, Nusse R. 1998. Wingless repression of *Drosophila* frizzled 2 expression shapes the Wingless morphogen gradient in the wing. *Cell* 93:767–777.
- Carroll SB. 1990. Zebra patterns in fly embryos: activation of stripes or repression of interstripes? *Cell* 60:9–16.
- Cavallo RA, Cox RT, Moline MM, Roose J, Poleyoy GA, Clevers H, Peifer M, Bejsovec A. 1998. *Drosophila* Tcf and Groucho interact to repress Wingless signalling activity. *Nature* 395:604–608.
- Chen CM, Struhl G. 1999. Wingless transduction by the Frizzled and Frizzled2 proteins of *Drosophila*. *Development* 126:5441–5452.
- Chen Y, Struhl G. 1996. Dual roles for patched in sequestering and transducing Hedgehog. *Cell* 87:553–563.
- Chen Y, Struhl G. 1998. In vivo evidence that Patched and Smoothened constitute distinct binding and transducing components of a Hedgehog receptor complex. *Development* 125:4943–4948.
- Chen Y, Gallaher N, Goodman RH, Smolik SM. 1998. Protein kinase A directly regulates the activity and proteolysis of cubitus interruptus. *Proc Natl Acad Sci U S A* 95:2349–2354.
- Chen Y, Goodman RH, Smolik SM. 2000. Cubitus interruptus requires *Drosophila* CREB-binding protein to activate wingless expression in the *Drosophila* embryo. *Mol Cell Biol* 20:1616–1625.
- Dawes R, Dawson I, Falciani F, Tear G, Akam M. 1994. Dax, a locust Hox gene related to fushi-tarazu but showing no pairwise expression. *Development* 120:1561–1572.

- Dearden PK, Akam M. 2001. Early embryo patterning in the grasshopper, *Schistocerca gregaria*: wingless, decapentaplegic and caudal expression. *Development* 128:3435–3444.
- Dierick HA, Bejsovec A. 1998. Functional analysis of Wingless reveals a link between intercellular ligand transport and dorsal-cell-specific signaling. *Development* 125:4729–4738.
- DiNardo S, Heemskerk J, Dougan S, O'Farrell PH. 1994. The making of a maggot: patterning the *Drosophila* embryonic epidermis. *Curr Opin Genet Dev* 4:529–534.
- DiNardo S, Sher E, Heemskerk-Jongens J, Kassis JA, O'Farrell PH. 1988. Two-tiered regulation of spatially patterned engrailed gene expression during *Drosophila* embryogenesis. *Nature* 332:604–609.
- Dominguez M, Brunner M, Hafen E, Basler K. 1996. Sending and receiving the hedgehog signal: control by the *Drosophila* Gli protein Cubitus interruptus. *Science* 272:1621–1625.
- Edgar BA, Odell GM, Schubiger G. 1989. A genetic switch, based on negative regulation, sharpens stripes in *Drosophila* embryos. *Dev Genet* 10:124–142.
- Gallitano-Mendel A, Finkelstein R. 1997. Novel segment polarity gene interactions during embryonic head development in *Drosophila*. *Dev Biol* 192:599–613.
- Gaul U, Jackle H. 1987. Pole region-dependent repression of the *Drosophila* gap gene Kruppel by maternal gene products. *Cell* 51:549–555.
- Gibson G, Wagner G. 2000. Canalization in evolutionary genetics: a stabilizing theory? *BioEssays* 22:372–380.
- Gonzalez F, Swales L, Bejsovec A, Skaer H, Martinez Arias A. 1991. Secretion and movement of wingless protein in the epidermis of the *Drosophila* embryo. *Mech Dev* 35:43–54.
- Grbic M, Nagy LM, Strand MR. 1998. Development of polyembryonic insects: a major departure from typical insect embryogenesis. *Dev Genes Evol* 208:69–81.
- Grossniklaus U, Pearson RK, Gehring WJ. 1992. The *Drosophila* sloppy paired locus encodes two proteins involved in segmentation that show homology to mammalian transcription factors. *Genes Dev* 6:1030–1051.
- Hacker U, Lin X, Perrimon N. 1997. The *Drosophila* sugarless gene modulates Wingless signaling and encodes an enzyme involved in polysaccharide biosynthesis. *Development* 124:3565–3573.
- Hartwell LH, Hopfield JJ, Leibler S, Murray AW. 1999. From molecular to modular cell biology. *Nature* 402: C47–52.
- Heemskerk J, DiNardo S, Kostriken R, O'Farrell PH. 1991. Multiple modes of engrailed regulation in the progression towards cell fate determination. *Nature* 352:404–410.
- Hepker J, Wang QT, Motzny CK, Holmgren R, Orenic TV. 1997. *Drosophila* cubitus interruptus forms a negative feedback loop with patched and regulates expression of Hedgehog target genes. *Development* 124:549–558.
- Hooper JE. 1994. Distinct pathways for autocrine and paracrine Wingless signalling in *Drosophila* embryos. *Nature* 372:461–464.
- Hooper JE, Scott MP. 1989. The *Drosophila* patched gene encodes a putative membrane protein required for segmental patterning. *Cell* 59:751–765.
- Ingham PW, Baker NE, Martinez-Arias A. 1988. Regulation of segment polarity genes in the *Drosophila* blastoderm by fushi tarazu and even skipped. *Nature* 331:73–75.
- Jiang J, Struhl G. 1998. Regulation of the Hedgehog and Wingless signalling pathways by the F-box/WD40-repeat protein Slimb. *Nature* 391:493–496.
- Keys DN, Lewis DL, Selegue JE, Pearson BJ, Goodrich LV, Johnson RL, Gates J, Scott MP, Carroll SB. 1999. Recruitment of a hedgehog regulatory circuit in butterfly eyespot evolution. *Science* 283:532–534.
- Kobayashi M, Tolkunova EN, Fujioka M, Jaynes JB. 1998. The role of extradenticle and Meis1/Homothorax as a mediator of Engrailed repression activity in embryos. *Annu Drosophila Res Conf Abstr*, 40th 184C.
- Kraut R, Levine M. 1991. Mutually repressive interactions between the gap genes giant and Kruppel define middle body regions of the *Drosophila* embryo. *Development* 111:611–621.
- Lawrence PA, Sampedro J. 1993. *Drosophila* segmentation: after the first three hours. *Development* 119:971–976.
- Lawrence PA, Casal J, Struhl G. 1999. hedgehog and engrailed: pattern formation and polarity in the *Drosophila* abdomen. *Development* 126:2431–2439.
- Lee HH, Frasch M. 2000. Wingless effects mesoderm patterning and ectoderm segmentation events via induction of its downstream target sloppy paired. *Development* 127: 5497–5508.
- Li X, Noll M. 1993. Role of the gooseberry gene in *Drosophila* embryos: maintenance of wingless expression by a wingless–gooseberry autoregulatory loop. *EMBO J* 12:4499–4509.
- Li X, Gutjahr T, Noll M. 1993. Separable regulatory elements mediate the establishment and maintenance of cell states by the *Drosophila* segment-polarity gene gooseberry. *EMBO J* 12:1427–1436.
- Lin X, Perrimon N. 1999. Dally cooperates with *Drosophila* Frizzled 2 to transduce Wingless signalling. *Nature* 400:281–284.
- Manoukian AS, Yoffe KB, Wilder EL, Perrimon N. 1995. The porcupine gene is required for wingless autoregulation in *Drosophila*. *Development* 121:4037–4044.
- Marigo V, Davey RA, Zuo Y, Cunningham JM, Tabin CJ. 1996. Biochemical evidence that patched is the Hedgehog receptor [see Comments]. *Nature* 384:176–179.
- Martinez-Arias A. 1993. Development and patterning of the larval epidermis of *Drosophila*. In: Bate M, Martinez-Arias A, editors. *The development of Drosophila melanogaster*. Plainview, NY: Cold Spring Harbor Laboratory Press. p 517–608.
- Martinez Arias A, Baker NE, Ingham PW. 1988. Role of segment polarity genes in the definition and maintenance of cell states in the *Drosophila* embryo. *Development* 103: 157–170.
- Meir E, von Dassow G, Munro E, Odell GM. 2002a. Robustness, flexibility, and the role of lateral inhibition in the neurogenic network. *Curr Biol* 12:778–786.
- Meir E, Munro E, Odell GM, von Dassow G. 2002b. Ingeneue: a versatile tool for reconstituting genetic networks, with examples from the segment polarity network. *J Exp Zool (Mol Dev Evol)* 294:216–251.
- Moline MM, Southern C, Bejsovec A. 1999. Directionality of wingless protein transport influences epidermal patterning in the *Drosophila* embryo. *Development* 126: 4375–4384.
- Monnier V, Dussillol F, Alves G, Lamour-Isnard C, Plessis A. 1998. Suppressor of fused links fused and Cubitus interruptus on the hedgehog signalling pathway. *Curr Biol* 8:583–586.
- Nagy LM. 1998. Changing patterns of gene regulation in the evolution of arthropod morphology. *Am Zool* 38: 818–828.

- Nagy LM, Carroll S. 1994. Conservation of wingless patterning functions in the short-germ embryos of *Tribolium castaneum*. *Nature* 367:460–463.
- Ohlmeier JT, Kalderon D. 1998. Hedgehog stimulates maturation of *Cubitus interruptus* into a labile transcriptional activator. *Nature* 396:749–753.
- Oppenheimer DI, MacNicol AM, Patel NH. 1999. Functional conservation of the wingless-engrailed interaction as shown by a widely applicable baculovirus misexpression system. *Curr Biol* 9:1288–1296.
- Orenic TV, Slusarski DC, Kroll KL, Holmgren RA. 1990. Cloning and characterization of the segment polarity gene *cubitus interruptus* Dominant of *Drosophila*. *Genes Dev* 4:1053–1067.
- Patel NH. 1994. The evolution of arthropod segmentation: insights from comparisons of gene expression patterns. *Development (Suppl)*:201–207.
- Patel NH, Martin-Blanco E, Coleman KG, Poole SJ, Ellis MC, Kornberg TB, Goodman CS. 1989. Expression of engrailed proteins in arthropods, annelids, and chordates. *Cell* 58:955–968.
- Patel NH, Ball EE, Goodman CS. 1992. Changing role of even-skipped during the evolution of insect pattern formation. *Nature* 357:339–342.
- Patel NH, Hayward DC, Lall S, Pirkel NR, DiPietro D, Ball EE. 2001. Grasshopper hunchback expression reveals conserved and novel aspects of axis formation and segmentation. *Development* 128:3459–3472.
- Peterson MD, Popadic A, Kaufman TC. 1998. The expression of two engrailed-related genes in an apterygote insect and a phylogenetic analysis of insect engrailed-related genes. *Dev Genes Evol* 208:547–557.
- Pfeiffer S, Vincent JP. 1999. Signalling at a distance: transport of Wingless in the embryonic epidermis of *Drosophila*. *Semin Cell Dev Biol* 10:303–309.
- Porter JA, Ekker SC, Park WJ, von Kessler DP, Young KE, Chen CH, Ma Y, Woods AS, Cotter RJ, Koonin EV, Beachy PA. 1996a. Hedgehog patterning activity: role of a lipophilic modification mediated by the carboxy-terminal autoprocessing domain. *Cell* 86:21–34.
- Porter JA, Young KE, Beachy PA. 1996b. Cholesterol modification of hedgehog signaling proteins in animal development. *Science* 274:255–259.
- Robbins DJ, Nybakken KE, Kobayashi R, Sisson JC, Bishop JM, Therond PP. 1997. Hedgehog elicits signal transduction by means of a large complex containing the kinesin-related protein *costal2*. *Cell* 90:225–234.
- Rogers BT, Kaufman TC. 1996. Structure of the insect head as revealed by the EN protein pattern in developing embryos. *Development* 122:3419–3432.
- Sanicola M, Sekelsky J, Elson S, Gelbart WM. 1995. Drawing a stripe in *Drosophila* imaginal disks: negative regulation of decapentaplegic and patched expression by engrailed. *Genetics* 139:745–756.
- Sanson B, Alexandre C, Fascetti N, Vincent JP. 1999. Engrailed and hedgehog make the range of Wingless asymmetric in *Drosophila* embryos. *Cell* 98:207–216.
- Sato A, Kojima T, Ui-Tei K, Miyata Y, Saigo K. 1999. Dfrizzled-3, a new *Drosophila* Wnt receptor, acting as an attenuator of Wingless signaling in wingless hypomorphic mutants. *Development* 126:4421–4430.
- Schmidt JE, von Dassow G, Kimelman D. 1996. Regulation of dorsal-ventral patterning: the ventralizing effects of the novel *Xenopus* homeobox gene *Vox*. *Development* 122:1711–1721.
- Schwartz C, Locke J, Nishida C, Kornberg TB. 1995. Analysis of *cubitus interruptus* regulation in *Drosophila* embryos and imaginal disks. *Development* 121:1625–1635.
- Sisson JC, Ho KS, Suyama K, Scott MP. 1997. *Costal2*, a novel kinesin-related protein in the Hedgehog signaling pathway. *Cell* 90:235–245.
- Sivasankaran R, Calleja M, Morata G, Basler K. 2000. The wingless target gene *dfz3* encodes a new member of the *Drosophila* frizzled family. *Mech Dev* 91:427–431.
- Sommer RJ, Tautz D. 1993. Involvement of an orthologue of the *Drosophila* pair-rule gene *hairy* in segment formation of the short germ-band embryo of *Tribolium* (Coleoptera). *Nature* 361:448–450.
- Strigini M, Cohen SM. 1997. A Hedgehog activity gradient contributes to AP axial patterning of the *Drosophila* wing. *Development* 124:4697–4705.
- Strigini M, Cohen SM. 2000. Wingless gradient formation in the *Drosophila* wing. *Curr Biol* 10:293–300.
- Struhl G, Barbash DA, Lawrence PA. 1997. Hedgehog organises the pattern and polarity of epidermal cells in the *Drosophila* abdomen. *Development* 124:2143–2154.
- Tabata T, Eaton S, Kornberg TB. 1992. The *Drosophila* hedgehog gene is expressed specifically in posterior compartment cells and is a target of engrailed regulation. *Genes Dev* 6:2635–2645.
- Tanaka K, Kitagawa Y, Kadowaki T. 2002. *Drosophila* segment polarity gene product porcupine stimulates the posttranslational N-glycosylation of wingless in the endoplasmic reticulum. *J Biol Chem* 277:12816–12823.
- Tautz D, Friedrich M, Schroder R. 1994. Insect embryogenesis—what is ancestral and what is derived? *Development (Suppl)*:193–199.
- The I, Perrimon N. 2000. Morphogen diffusion: the case of the Wingless protein. *Nat Cell Biol* 2:E79–E82.
- Therond PP, Limbourg Bouchon B, Gallet A, Dussilol F, Pietri T, van den Heuvel M, Tricoire H. 1999. Differential requirements of the Fused kinase for Hedgehog signalling in the *Drosophila* embryo. *Development* 126:4039–4051.
- Tsuda M, Kamimura K, Nakato H, Archer M, Staatz W, Fox B, Humphrey M, Olson S, Futch T, Kaluza V, Siegfried E, Stam L, Selleck SB. 1999. The cell-surface proteoglycan Dally regulates Wingless signalling in *Drosophila*. *Nature* 400:276–280.
- van de Wetering M, Cavallo R, Dooijes D, van Beest M, van Es J, Loureiro J, Ypma A, Hursh D, Jones T, Bejsovec A, Peifer M, Mortin M, Clevers H. 1997. Armadillo coactivates transcription driven by the product of the *Drosophila* segment polarity gene *dTCF*. *Cell* 88:789–799.
- van den Heuvel M, Ingham PW. 1996. *smoothed* encodes a receptor-like serpentine protein required for hedgehog signalling. *Nature* 382:547–551.
- van den Heuvel M, Nusse R, Johnston P, Lawrence PA. 1989. Distribution of the wingless gene product in *Drosophila* embryos: a protein involved in cell-cell communication. *Cell* 59:739–749.
- Vincent JP, Lawrence PA. 1994. *Drosophila* wingless sustains engrailed expression only in adjoining cells: evidence from mosaic embryos. *Cell* 77:909–915.
- Vincent JP, O'Farrell PH. 1992. The state of engrailed expression is not clonally transmitted during early *Drosophila* development. *Cell* 68:923–931.
- Vinson CR, Conover S, Adler PN. 1989. A *Drosophila* tissue polarity locus encodes a protein containing seven potential transmembrane domains. *Nature* 338:263–264.

- von Dassow G, Munro E. 1999. Modularity in animal development and evolution: elements of a conceptual framework for EvoDevo. *J Exp Zool (Mol Dev Evol)* 285:307–325.
- von Dassow G, Schmidt JE, Kimelman D. 1993. Induction of the *Xenopus* organizer: expression and regulation of Xnot, a novel FGF and activin-regulated homeo box gene. *Genes Dev* 7:355–366.
- von Dassow G, Meir E, Munro EM, Odell GM. 2000. The segment polarity network is a robust developmental module. *Nature* 406:188–192.
- Von Ohlen T, Hooper JE. 1997. Hedgehog signaling regulates transcription through Gli/Ci binding sites in the wingless enhancer. *Mech Dev* 68:149–156.
- Von Ohlen T, Lessing D, Nusse R, Hooper JE. 1997. Hedgehog signaling regulates transcription through cubitus interruptus, a sequence-specific DNA binding protein. *Proc Natl Acad Sci U S A* 94:2404–2409.
- Wagner GP, Booth G, Bagheri-Chaichian H. 1997. A population genetic theory of canalization. *Evolution* 51:329–347.
- Waltzer L, Bienz M. 1998. *Drosophila* CBP represses the transcription factor TCF to antagonize Wingless signalling. *Nature* 395:521–525.
- Wang QT, Holmgren RA. 1999. The subcellular localization and activity of *Drosophila* cubitus interruptus are regulated at multiple levels. *Development* 126:5097–5106.
- Wesley CS. 1999. Notch and wingless regulate expression of cuticle patterning genes. *Mol Cell Biol* 19:5743–5758.
- Yoffe KB, Manoukian AS, Wilder EL, Brand AH, Perrimon N. 1995. Evidence for engrailed-independent wingless auto-regulation in *Drosophila*. *Dev Biol* 170:636–650.

### MATHEMATICAL APPENDIX

Each of the models described in this paper consists of a system of coupled ordinary differential equations, assembled and solved by the computer program Ingeneue (described in companion paper by Meir et al., '02, this issue). In this section we use the following short-hand:

$$\phi(X, \kappa_X, \nu_X) = \left( \frac{X^{\nu_X}}{\kappa_X^{\nu_X} + X^{\nu_X}} \right), \quad (1)$$

$$\psi(X, \kappa_X, \nu_X) = 1 - \phi(X, \kappa_X, \nu_X), \quad (2)$$

$X_{i,j}$  = amount of  $X$  on cell  $i$ , face  $j$ ;

$n(i,j)$  = index of neighbor to cell  $i$  at face  $j$ ;

$X_{n(i,j)j+3}$  =  $X$  on cell face apposite to  $i,j$ ;

$$X_i^{tot} = \sum_{j=1}^6 X_{i,j} = \text{total } X \text{ in cell } i;$$

$$X_{n(i,j)}^{tot} = \sum_{j=1}^6 X_{n(i,j)j+3} = \text{total } X \text{ presented to cell } i \text{ by neighbors.}$$

All equations in this appendix are presented in the dimensionless form used by Ingeneue and explained in the supplement to von Dassow et al. ('00). In Ingeneue each process (transcription, cleavage, first-order decay, ligand binding, etc.) must be represented as a single additive term. Below, equations correspond directly to the script used by Ingeneue, except that for brevity and convenience we group terms differently.

The model referred to as “spg1” is identical to the model described in that paper, and consists of the following equations, instantiated across an arbitrary-size cell grid (enumerated by the index  $i$  below):

$$\frac{d en_i}{d\tau} = \frac{T_o}{H_{en}} \left( \phi \left( EWG_{n(i,j)}^{tot} \cdot \psi(CN_i, \kappa_{CNen}, \nu_{CNen}), \kappa_{WGen}, \nu_{WGen} \right) - en_i \right), \quad (3)$$

$$\frac{d EN_i}{d\tau} = \frac{T_o}{H_{EN}} (en_i - EN_i), \quad (4)$$

$$\begin{aligned} \frac{d wg_i}{d\tau} = & \frac{T_o}{H_{wg}} \left( \frac{\alpha_{CIwg} \cdot \phi(CI_i \cdot \psi(CN_i, \kappa_{CNwg}, \nu_{CNwg}), \kappa_{CIwg}, \nu_{CIwg}) + \alpha_{WGwg} \cdot \phi(IWG_i, \kappa_{WGwg}, \nu_{WGwg})}{1 + \alpha_{CIwg} \cdot \phi(CI_i \cdot \psi(CN_i, \kappa_{CNwg}, \nu_{CNwg}), \kappa_{CIwg}, \nu_{CIwg}) + \alpha_{WGwg} \cdot \phi(IWG_i, \kappa_{WGwg}, \nu_{WGwg})} \right) \\ & - \frac{T_o wg_i}{H_{wg}}, \end{aligned} \quad (5)$$



$$\frac{dIWG_i}{d\tau} = \frac{T_o}{H_{IWG}} (wg_i - IWG_i) + T_o (r_{EndoWG} EWG_i^{tot} - r_{ExoWG} IWG_i), \quad (6)$$

$$\frac{dEWG_{i,j}}{d\tau} = T_o \left( \begin{array}{c} \frac{r_{ExoWG} IWG_i}{6} - r_{EndoWG} EWG_{i,j} + \\ r_{MxferWG} (EWG_{n(i,j),j+3} - EWG_{i,j}) + \\ r_{LMxferWG} (EWG_{i,j-1} + EWG_{i,j+1} - 2EWG_{i,j}) \end{array} \right) - \frac{T_o EWG_{i,j}}{H_{IWG}}, \quad (7)$$

$$\frac{dptc_i}{d\tau} = \frac{T_o}{H_{ptc}} (\phi(CI_i \cdot \psi(CN_i, \kappa_{CNptc}, \nu_{CNptc}), \kappa_{CIptc}, \nu_{CIptc}) - ptc_i) \quad (8)$$

$$\begin{aligned} \frac{dPTC_{i,j}}{d\tau} &= \frac{T_o}{H_{PTC}} \left( \frac{ptc_i}{6} - PTC_{i,j} \right) - T_o k_{PTCHH} [HH]_o HH_{n(i,j),j+3} \cdot PTC_{i,j} \\ &+ T_o r_{LMxferPTC} (PTC_{i,j-1} + PTC_{i,j+1} - 2PTC_{i,j}), \end{aligned} \quad (9)$$

$$\frac{dci_i}{d\tau} = \frac{T_o}{H_{ci}} (\phi(B_i \cdot \psi(EN_i, \kappa_{ENci}, \nu_{ENci}), \kappa_{Bci}, \nu_{Bci}) - ci_i), \quad (10)$$

$$\frac{dCI_i}{d\tau} = \frac{T_o}{H_{CI}} (ci_i - CI_i) - T_o C_{CI} CI_i \cdot \phi(PTC_i^{tot}, \kappa_{PTC.CI}, \nu_{PTC.CI}), \quad (11)$$

$$\frac{dCN_i}{d\tau} = T_o C_{CI} CI_i \cdot \phi(PTC_i^{tot}, \kappa_{PTC.CI}, \nu_{PTC.CI}) - \frac{T_o CN_i}{H_{CI}} \quad (12)$$

$$\frac{dhh_i}{d\tau} = \frac{T_o}{H_{hh}} (\phi(EN_i \cdot \psi(CN_i, \kappa_{CNhh}, \nu_{CNhh}), \kappa_{ENhh}, \nu_{ENhh}) - hh_i), \quad (13)$$

$$\begin{aligned} \frac{dHH_{i,j}}{d\tau} &= \frac{T_o}{H_{HH}} \left( \frac{hh_i}{6} - HH_{i,j} \right) - T_o k_{PTCHH} [PTC]_o PTC_{n(i,j),j+3} \cdot HH_{i,j} \\ &+ T_o r_{LMxferHH} (HH_{i,j-1} + HH_{i,j+1} - 2HH_{i,j}), \end{aligned} \quad (14)$$

$$\frac{dPH_{i,j}}{d\tau} = T_o k_{PTCHH} [HH]_o HH_{n(i,j),j+3} \cdot PTC_{i,j} - \frac{T_o PH_{i,j}}{H_{PH}}. \quad (15)$$

In Section II we described re-wiring spg1 in several ways. For example, adding inhibition of *ptc* transcription by En amounts to replacing Eq. (8) above with

$$\frac{dptc_i}{d\tau} = \frac{T_o}{H_{ptc}} (\phi(CI_i \cdot \psi(CN_i, \kappa_{CNptc}, \nu_{CNptc}), \kappa_{CIptc}, \nu_{CIptc}) \cdot \psi(EN_i, \kappa_{ENptc}, \nu_{ENptc}) - ptc_i). \quad (16)$$

For another example, to introduce the products of the gene *slp*, as in line 14 in Table 3, we add the equations

$$\frac{dslp_i}{d\tau} = \frac{T_o}{H_{slp}} (\phi(EWG_i^{tot} \cdot \psi(EN_i, \kappa_{ENslp}, \nu_{ENslp}), (\kappa_{WGslp}, \nu_{WGslp}) - slp_i), \quad (17)$$

$$\frac{dSLP_i}{d\tau} = \frac{T_o}{H_{SLP}} (slp_i - SLP_i). \quad (18)$$

In addition we modify the equations for *en* and *wg*, replacing Eqs. (3) and (5) as follows:

$$\frac{den_i}{d\tau} = \frac{T_o}{H_{en}} (\phi(EWG_i^{tot} \cdot \psi(CN_i, \kappa_{CNen}, \nu_{CNen}), \kappa_{WGen}, \nu_{WGen}) \cdot \psi(SLP_i, \kappa_{SLPen}, \nu_{SLPen}) - en_i), \quad (19)$$

$$\begin{aligned} \frac{dwg_i}{d\tau} &= \frac{T_o}{H_{wg}} \left( \frac{\alpha_{CIwg} \cdot \phi(CI_i \cdot \psi(CN_i, \kappa_{CNwg}, \nu_{CNwg}), \kappa_{CIwg}, \nu_{CIwg}) + \alpha_{SLPwg} \cdot \phi(SLP_i, \kappa_{SLPwg}, \nu_{SLPwg})}{1 + \alpha_{CIwg} \cdot \phi(CI_i \cdot \psi(CN_i, \kappa_{CNwg}, \nu_{CNwg}), \kappa_{CIwg}, \nu_{CIwg}) + \alpha_{SLPwg} \cdot \phi(SLP_i, \kappa_{SLPwg}, \nu_{SLPwg})} \right) \\ &- \frac{T_o wg_i}{H_{wg}}. \end{aligned} \quad (20)$$

Naturally this represents just one of the many ways which one could introduce the new Nodes and links. Equations (5) and (20) both express an additive relationship between the positive influences on  $wg$  transcription. In Section IV we show that such a format makes it very difficult to find parameters that enable the stripe of  $wg$ -expressing cells to sharpen into a single-cell-wide row. An alternate, synergistic formulation that enables  $wg$  stripe sharpening corresponds to replacing Eq. (5) with

$$\frac{dwg_i}{d\tau} = \frac{T_o}{H_{wg}} (\phi(CI_i \cdot \psi(CN_i, \kappa_{CNwg}, \nu_{CNwg}), \kappa_{CIwg}, \nu_{CIwg}) \cdot \phi(IWG_i, \kappa_{WGwg}, \nu_{WGwg}) - wg_i). \quad (21)$$

More complex versions of the model, such as `spg2` and `spg4`, are derived in the same way, by adding extra Nodes and modifying various additive terms as needed. For example, the model “`spg2`”, Variant E (see Fig. 10 and Table 4), consists of the following equations:

$$\frac{den_i}{d\tau} = \frac{T_o}{H_{en}} (\phi(AP_i \cdot \psi(CN_i, \kappa_{CNen}, \nu_{CNen}), \kappa_{APen}, \nu_{APen}) - en_i), \quad (22)$$

$$\frac{dEN_i}{d\tau} = \frac{T_o}{H_{EN}} (en_i - EN_i), \quad (23)$$

$$\begin{aligned} \frac{dwg_i}{d\tau} = & \frac{T_o}{H_{wg}} \left( \frac{\alpha_{CIwg} \cdot \phi(CI_i \cdot \psi(CN_i, \kappa_{CNwg}, \nu_{CNwg}), \kappa_{CIwg}, \nu_{CIwg}) + \alpha_{WGwg} \cdot \phi(IWG_i, \kappa_{WGwg}, \nu_{WGwg})}{1 + \alpha_{CIwg} \cdot \phi(CI_i \cdot \psi(CN_i, \kappa_{CNwg}, \nu_{CNwg}), \kappa_{CIwg}, \nu_{CIwg}) + \alpha_{WGwg} \cdot \phi(IWG_i, \kappa_{WGwg}, \nu_{WGwg})} \right) \\ & - \frac{T_o \cdot wg_i}{H_{wg}}, \end{aligned} \quad (24)$$

$$\frac{dIWG_i}{d\tau} = \frac{T_o}{H_{IWG}} (wg_i - IWG_i) + T_o (r_{EndoWG} EWG_i^{tot} - r_{ExoWG} IWG_i), \quad (25)$$

$$\frac{dEWG_{i,j}}{d\tau} = T_o \left( \begin{array}{c} \frac{r_{ExoWG} IWG_i}{6} - r_{EndoWG} EWG_{i,j} + \\ r_{MxferWG} (EWG_{n(i,j)j+3} - EWG_{i,j}) + \\ r_{LMxferWG} (EWG_{i,j-1} + EWG_{i,j+1} - 2EWG_{i,j}) - \\ T_o k_{FZWG} [FZ]_o FZ_{i,j} \cdot EWG_{i,j} \end{array} \right) - \frac{T_o EWG_{i,j}}{H_{IWG}}, \quad (26)$$

$$\frac{dfz_i}{d\tau} = \frac{T_o}{H_{fz}} (\phi(PAN_i \cdot \psi(AP_i, \kappa_{APfz}, \nu_{APfz}), \kappa_{PANfz}, \nu_{PANfz}) - fz_i), \quad (27)$$

$$\begin{aligned} \frac{dFZ_{i,j}}{d\tau} = & \frac{T_o}{H_{FZ}} \left( \frac{fz_i}{6} - FZ_{i,j} \right) \\ & - T_o k_{FZWG} [EWG]_o EWG_{i,j} \cdot FZ_{i,j} + T_o r_{LMxferFZ} (FZ_{i,j-1} + FZ_{i,j+1} - 2FZ_{i,j}), \end{aligned} \quad (28)$$

$$\frac{dFW_{i,j}}{d\tau} = T_o k_{FZWG} [EWG]_o EWG_{i,j} \cdot FZ_{i,j} + T_o r_{LMxferFW} (FW_{i,j-1} + FW_{i,j+1} - 2FW_{i,j}) - \frac{T_o FW_{i,j}}{H_{FW}}, \quad (29)$$

$$\frac{darm_i}{d\tau} = \frac{T_o}{H_{arm}} (\phi(B_i, \kappa_{Barm}, \nu_{Barm}) - arm_i), \quad (30)$$

$$\begin{aligned} \frac{dARM_i}{d\tau} = & \frac{T_o}{H_{ARM}} (arm_i - ARM_i) \\ & - T_o C_{ARM} ARM_i \cdot \psi(FW_i^{tot}, \kappa_{FW.ARM}, \nu_{FW.ARM}) - T_o k_{ARMPAN} [PAN]_o PAN_i \cdot ARM_i, \end{aligned} \quad (31)$$

$$\frac{dpan_i}{d\tau} = \frac{T_o}{H_{pan}} (\phi(B_i, \kappa_{Bpan}, \nu_{Bpan}) - pan_i), \quad (32)$$

$$\frac{dPAN_i}{d\tau} = \frac{T_o}{H_{PAN}} (pan_i - PAN_i) - T_o k_{ARMPAN} [ARM]_o ARM_i \cdot PAN_i, \quad (33)$$

$$\frac{dAP_i}{d\tau} = T_o k_{ARMPAN}[PAN]_o PAN_i \cdot ARM_i - \frac{T_o AP_i}{H_{AP}}, \quad (34)$$

$$\frac{dptc_i}{d\tau} = \frac{T_o}{H_{ptc}} \left( \phi(CI_i \cdot \psi(CN_i, \kappa_{CNptc}, \nu_{CNptc}), \kappa_{CIptc}, \nu_{CIptc}) - ptc_i \right), \quad (35)$$

$$\begin{aligned} \frac{dPTC_{i,j}}{d\tau} = & \frac{T_o}{H_{PTC}} \left( \frac{ptc_i}{6} - PTC_{i,j} \right) \\ & - T_o k_{PTCHH}[HH]_o HH_{n(i,j)j+3} \cdot PTC_{i,j} + T_o r_{LMxferPTC} (PTC_{i,j-1} + PTC_{i,j+1} - 2PTC_{i,j}), \end{aligned} \quad (36)$$

$$\frac{dci_i}{d\tau} = \frac{T_o}{H_{ci}} \left( \phi(B_i \cdot \psi(EN_i, \kappa_{ENci}, \nu_{ENci}), \kappa_{Bci}, \nu_{Bci}) - ci_i \right), \quad (37)$$

$$\frac{dCI_i}{d\tau} = \frac{T_o}{H_{CI}} (ci_i - CI_i) - T_o C_{CI} CI_i \cdot \phi(PTC_i^{tot}, \kappa_{PTC.CI}, \nu_{PTC.CI}), \quad (38)$$

$$\frac{dCN_i}{d\tau} = T_o C_{CI} CI_i \cdot \phi(PTC_i^{tot}, \kappa_{PTC.CI}, \nu_{PTC.CI}) - \frac{T_o CN_i}{H_{CI}}, \quad (39)$$

$$\frac{dhh_i}{d\tau} = \frac{T_o}{H_{hh}} \left( \phi(EN_i \cdot \psi(CN_i, \kappa_{CNhh}, \nu_{CNhh}), \kappa_{ENhh}, \nu_{ENhh}) - hh_i \right), \quad (40)$$

$$\begin{aligned} \frac{dHH_{i,j}}{d\tau} = & \frac{T_o}{H_{HH}} \left( \frac{hh_i}{6} - HH_{i,j} \right) \\ & - T_o k_{PTCHH}[PTC]_o PTC_{n(i,j)j+3} \cdot HH_{i,j} + T_o r_{LMxferHH} (HH_{i,j-1} + HH_{i,j+1} - 2HH_{i,j}), \end{aligned} \quad (41)$$

$$\frac{dPH_{i,j}}{d\tau} = T_o k_{PTCHH}[HH]_o HH_{n(i,j)j+3} \cdot PTC_{i,j} - \frac{T_o PH_{i,j}}{H_{PH}}. \quad (42)$$

A subset of the network including only *en*, *slp*, and *wg* (described in Fig. 6 of the companion paper) is represented by the following equations:

$$\frac{den_i}{d\tau} = \frac{T_o}{H_{en}} \left( \phi(WG_i^{tot}, \kappa_{WGen}, \nu_{WGen}) \cdot \psi(SLP_i, \kappa_{SLPen}, \nu_{SLPen}) - en_i \right), \quad (43)$$

$$\frac{dEN_i}{d\tau} = \frac{T_o}{H_{EN}} (en_i - EN_i), \quad (44)$$

$$\frac{dslp_i}{d\tau} = \frac{T_o}{H_{slp}} \left( \phi(WG_i^{tot}, \kappa_{WGslp}, \nu_{WGslp}) \cdot \psi(EN_i, \kappa_{ENslp}, \nu_{ENslp}) - slp_i \right), \quad (45)$$

$$\frac{dSLP_i}{d\tau} = \frac{T_o}{H_{SLP}} (slp_i - SLP_i), \quad (46)$$

$$\frac{d wg_i}{d\tau} = \frac{T_o}{H_{wg}} \left( \phi(SLP_i, \kappa_{SLPwg}, \nu_{SLPwg}) - wg_i \right), \quad (47)$$

$$\frac{dWG_{i,j}}{d\tau} = \frac{T_o}{H_{WG}} \left( \frac{wg_i}{6} - WG_{i,j} \right) + T_o (r_{MxferWG} (WG_{n(i,j)j+3} - WG_{i,j}) + r_{LMxferWG} (WG_{i,j-1} + WG_{i,j+1} - 2WG_{i,j})). \quad (48)$$

Another simplified model used Section III of this paper collapses Nodes representing mRNA and protein into a single Node for each locus:

$$\frac{dEN_i}{d\tau} = \frac{T_o}{H_{EN}} \left( \phi(EWG_{n(i,j)}^{tot} \cdot \psi(CN_i, \kappa_{CNen}, \nu_{CNen}), \kappa_{WGen}, \nu_{WGen}) - EN_i \right), \quad (49)$$

$$\begin{aligned} \frac{dIWG_i}{d\tau} = & \frac{T_o}{H_{IWG}} \left( \frac{\alpha_{CIwg} \cdot \phi(CI_i \cdot \psi(CN_i, \kappa_{CNwg}, \nu_{CNwg}), \kappa_{CIwg}, \nu_{CIwg}) + \alpha_{WGwg} \cdot \phi(IWG_i, \kappa_{WGwg}, \nu_{WGwg})}{1 + \alpha_{CIwg} \cdot \phi(CI_i \cdot \psi(CN_i, \kappa_{CNwg}, \nu_{CNwg}), \kappa_{CIwg}, \nu_{CIwg}) + \alpha_{WGwg} \cdot \phi(IWG_i, \kappa_{WGwg}, \nu_{WGwg})} \right) \\ & - \frac{T_o IWG_i}{H_{IWG}} + T_o (r_{EndoWG} EWG_i^{tot} - r_{ExoWG} IWG_i), \end{aligned} \quad (50)$$

$$\frac{dEWG_{i,j}}{d\tau} = T_o \left( \begin{array}{c} \frac{r_{ExoWG} IWG_i}{6} - r_{EndoWG} EWG_{i,j} + \\ r_{MxferWG} (EWG_{n(i,j)j+3} - EWG_{i,j}) + \\ r_{LMxferWG} (EWG_{i,j-1} + EWG_{i,j+1} - 2EWG_{i,j}) \end{array} \right) - \frac{T_o EWG_{i,j}}{H_{IWG}}, \quad (51)$$

$$\begin{aligned} \frac{dPTC_{i,j}}{d\tau} = & \frac{T_o}{H_{PTC}} \left( \frac{\phi(CI_i \cdot \psi(CN_i, \kappa_{CNptc}, \nu_{CNptc}), \kappa_{CIptc}, \nu_{CIptc})}{6} - PTC_{i,j} \right) \\ & - T_o k_{PTCHH} [HH]_o HH_{n(i,j)j+3} \cdot PTC_{i,j} + T_o r_{LMxferPTC} (PTC_{i,j-1} + PTC_{i,j+1} - 2PTC_{i,j}), \end{aligned} \quad (52)$$

$$\frac{dCI_i}{d\tau} = \frac{T_o}{H_{CI}} (\phi(B_i \cdot \psi(EN_i, \kappa_{ENci}, \nu_{ENci}), \kappa_{Bci}, \nu_{Bci}) - CI_i) - T_o C_{CI} CI_i \cdot \phi(PTC_i^{tot}, \kappa_{PTC.CI}, \nu_{PTC.CI}), \quad (53)$$

$$\frac{dCN_i}{d\tau} = T_o C_{CI} CI_i \cdot \phi(PTC_i^{tot}, \kappa_{PTC.CI}, \nu_{PTC.CI}) - \frac{T_o CN_i}{H_{CI}}, \quad (54)$$

$$\begin{aligned} \frac{dHH_{i,j}}{d\tau} = & \frac{T_o}{H_{HH}} \left( \frac{\phi(EN_i \cdot \psi(CN_i, \kappa_{CNhh}, \nu_{CNhh}), \kappa_{ENhh}, \nu_{ENhh})}{6} - HH_{i,j} \right) \\ & - T_o k_{PTCHH} [PTC]_o PTC_{n(i,j)j+3} \cdot HH_{i,j} + T_o r_{LMxferHH} (HH_{i,j-1} + HH_{i,j+1} - 2HH_{i,j}), \end{aligned} \quad (55)$$

$$\frac{dPH_{i,j}}{d\tau} = T_o k_{PTCHH} [HH]_o HH_{n(i,j)j+3} \cdot PTC_{i,j} - \frac{T_o PH_{i,j}}{H_{PH}}. \quad (56)$$

Notice that Eqs. (49–56) consist largely of the same terms as Eqs. (3–15). In the original model, the two processes of translation and first-order non-specific decay cause each (scaled) protein concentration to track the mRNA concentration at a rate determined by the protein’s half-life. In the segment polarity models, most proteins undergo additional transformations; however En does not. Equation (4), governing EN concentration, is a simple tracking function (likewise for Eq. (23), in *spg2*). The non-dimensionalization recipe we use reveals that the half-life of each molecular species determines how long that species takes to decline *or accumulate* to steady-state concentration. The half-lives thus govern the timescale on which Nodes respond to any perturbations at the biosynthetic level. The difference between the collapsed version in Eqs. (49–56) and our “normal” form, in which mRNA and protein are separate species, is the elimination of this dampening layer. In the normal form, if the protein’s half-life is longer than the mRNA’s half-life, separation into two (or more) steps insulates the concentration of functional product (protein) from fluctuations in the level of transcriptional stimulus. The collapsed network consequently can work, but, more often than the original network, fails to hold a stable steady state in the face of oscillations generated within the *ci-ptc* negative feedback loop. The real process of gene expression is broken into many intermediate steps, as are metabolic pathways, and one wonders if evolution has exploited the oscillation-damping effect of intermediate steps with slower response times to insulate biochemical networks against stochastic variability.

Finally, in Section III we compared networks “inspired by actual events” to a simple network of our own concoction, which is described by the following equations governing the products of two hypothetical genes called A and B:

$$\frac{da_i}{d\tau} = \frac{T_o}{H_a} (\phi(AB_i^{tot} \cdot \psi(B_{n(i,j)}^{tot}, \kappa_{Ba}, \nu_{Ba}), \kappa_{ABa}, \nu_{ABa}) \cdot \phi(A_i, \kappa_{Aa}, \nu_{Aa}) - a_i), \quad (57)$$

$$\frac{dA_{ij}}{d\tau} = \frac{T_{\circ}}{H_A} \left( \frac{a_i}{6} - A_{ij} \right) + T_{\circ} \left( \begin{array}{c} k_{AB \rightarrow A+B} \frac{[B]_{\circ}}{[A]_{\circ}} AB_{ij} - k_{A+B \rightarrow AB} [B]_{\circ} B_{ij} \cdot A_{ij} \\ + r_{MxferA} (A_{n(i,j),j+3} - A_{ij}) + r_{LMxferA} (A_{i,j-1} + A_{i,j+1} - 2A_{ij}) \end{array} \right), \quad (58)$$

$$\frac{db_i}{d\tau} = \frac{T_{\circ}}{H_b} \left( \phi(AB_i^{tot} \cdot \psi(A_{n(i,j)}^{tot}, \kappa_{Ab}, \nu_{Ab}), \kappa_{ABb}, \nu_{ABb}) \cdot \phi(B_i, \kappa_{Bb}, \nu_{Bb}) - b_i \right), \quad (59)$$

$$\frac{dB_{ij}}{d\tau} = \frac{T_{\circ}}{H_B} \left( \frac{b_i}{6} - B_{ij} \right) + T_{\circ} \left( \begin{array}{c} k_{AB \rightarrow A+B} AB_{ij} - k_{A+B \rightarrow AB} [A]_{\circ} A_{ij} \cdot B_{ij} \\ + r_{MxferB} (B_{n(i,j),j+3} - B_{ij}) + r_{LMxferB} (B_{i,j-1} + B_{i,j+1} - 2B_{ij}) \end{array} \right), \quad (60)$$

$$\frac{dAB_{ij}}{d\tau} = -\frac{T_{\circ} AB_{ij}}{H_{AB}} + T_{\circ} \left( \begin{array}{c} k_{A+B \rightarrow AB} [A]_{\circ} A_{ij} \cdot B_{ij} - k_{AB \rightarrow A+B} AB_{ij} \\ + r_{MxferAB} (AB_{n(i,j),j+3} - AB_{ij}) + r_{LMxferAB} (AB_{i,j-1} + AB_{i,j+1} - 2AB_{ij}) \end{array} \right). \quad (61)$$

This network is entirely fictional. Any resemblance to real networks, living or dead, is accidental. Note that the term for dissociation in the equation governing A is scaled by the ratio of the maximum attainable concentrations of A and B ( $[A]_{\circ}/[B]_{\circ}$ ) to make the non-dimensionalization scheme work out; otherwise the imaginary components A and B are symmetric with respect to their interactions and transcriptional control, but can differ quantitatively because they are governed by independent parameters. If their various parameters are likewise forced to be symmetrically valued, then  $[A]_{\circ}/[B]_{\circ}=1$ .